Cell Reports

Article

Nuclear Import Receptors Directly Bind to Arginine-Rich Dipeptide Repeat Proteins and Suppress Their Pathological Interactions

Graphical Abstract

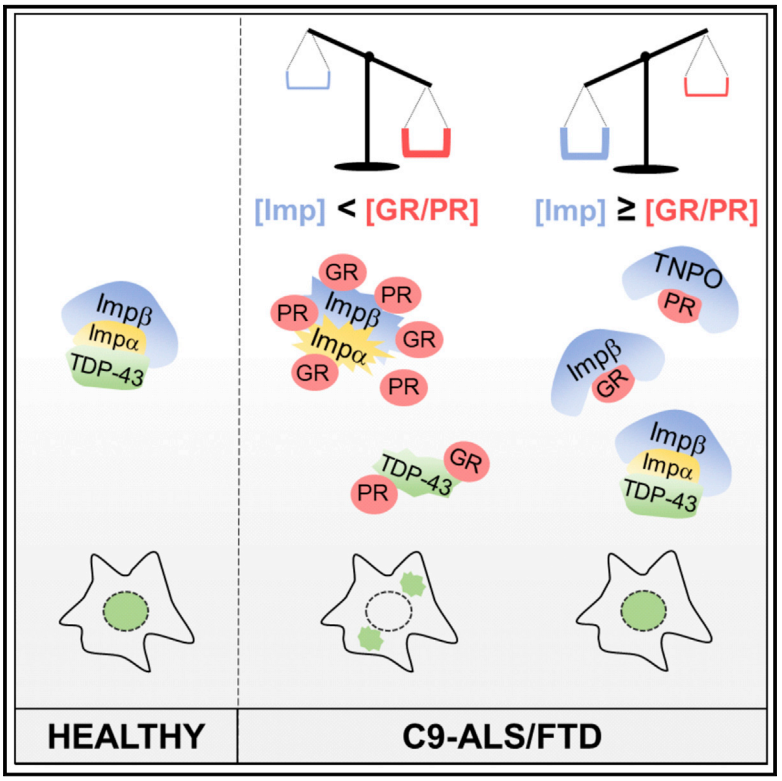

Highlights

- Importins directly bind to arginine-rich dipeptide repeat proteins (R-rich DPRs)
- R-rich DPRs induce importin and TDP-43 condensation
- Poly-GR impairs TDP-43 nuclear import
- Elevated importin levels shield R-rich DPRs from pathological interactions

Authors

Saskia Hutten, Sinem Usluer, Benjamin Bourgeois, ..., Dieter Edbauer, Tobias Madl, Dorothee Dormann

Correspondence

saskia.hutten@med.uni-muenchen.de (S.H.), dorothee.dormann@med.uni-muenchen.de (D.D.)

In Brief

Hutten et al. show that arginine-rich dipeptide repeat proteins (DPRs) associated with the neurodegenerative diseases ALS and FTD bind directly to importins, promote their condensation, and interfere with importin function. Elevated importin levels can shield arginine-rich DPRs and suppress DPR-induced phase separation of TDP-43 and RNA.

Hutten et al., 2020, Cell Reports *33*, 108538
December 22, 2020
https://doi.org/10.1016/j.celrep.2020.108538

CellPress

Cell Reports

CellPress
OPEN ACCESS

Article

Nuclear Import Receptors Directly Bind to Arginine-Rich Dipeptide Repeat Proteins and Suppress Their Pathological Interactions

Saskia Hutten,[1,*] Sinem Usluer,[3] Benjamin Bourgeois,[3] Francesca Simonetti,[1] Hana M. Odeh,[4] Charlotte M. Fare,[4,5] Mareike Czuppa,[6] Marian Hruska-Plochan,[2] Mario Hofweber,[1,8] Magdalini Polymenidou,[2] James Shorter,[4,5] Dieter Edbauer,[6,8,9] Tobias Madl,[3,7] and Dorothee Dormann[1,8,9,10,*]

[1]BioMedical Center (BMC), Ludwig-Maximilians-University Munich, 82152 Planegg-Martinsried, Germany
[2]Department of Quantitative Biomedicine, University of Zurich, Winterthurerstrasse 190, 8057 Zurich, Switzerland
[3]Gottfried Schatz Research Center for Cell Signaling, Metabolism and Aging, Molecular Biology & Biochemistry, Medical University of Graz, 8010 Graz, Austria
[4]Department of Biochemistry and Biophysics, Perelman School of Medicine, University of Pennsylvania, Philadelphia, PA 19104, USA
[5]Biochemistry and Molecular Biophysics Graduate Group, Perelman School of Medicine at the University of Pennsylvania, Philadelphia, PA 19104, USA
[6]German Center for Neurodegenerative Diseases (DZNE), Munich, Feodor-Lynen-Str. 17, 81377 Munich, Germany
[7]BioTechMed-Graz, 8010 Graz, Austria
[8]LMU Graduate School of Systemic Neurosciences (GSN), 82152 Planegg-Martinsried, Germany
[9]Munich Cluster for Systems Neurology (SyNergy), 81377 Munich, Germany
[10]Lead Contact
*Correspondence: saskia.hutten@med.uni-muenchen.de (S.H.), dorothee.dormann@med.uni-muenchen.de (D.D.)
https://doi.org/10.1016/j.celrep.2020.108538

SUMMARY

Nuclear import receptors, also called importins, mediate nuclear import of proteins and chaperone aggregation-prone cargoes (e.g., neurodegeneration-linked RNA-binding proteins [RBPs]) in the cytoplasm. Importins were identified as modulators of cellular toxicity elicited by arginine-rich dipeptide repeat proteins (DPRs), an aberrant protein species found in *C9orf72*-linked amyotrophic lateral sclerosis (ALS) and frontotemporal dementia (FTD). Mechanistically, the link between importins and arginine-rich DPRs remains unclear. Here, we show that arginine-rich DPRs (poly-GR and poly-PR) bind directly to multiple importins and, in excess, promote their insolubility and condensation. In cells, poly-GR impairs Impα/β-mediated nuclear import, including import of TDP-43, an RBP that aggregates in *C9orf72*-ALS/FTD patients. Arginine-rich DPRs promote phase separation and insolubility of TDP-43 *in vitro* and in cells, and this pathological interaction is suppressed by elevating importin concentrations. Our findings suggest that importins can decrease toxicity of arginine-rich DPRs by suppressing their pathological interactions.

INTRODUCTION

Amyotrophic lateral sclerosis (ALS) and frontotemporal dementia (FTD) are progressive and eventually fatal neurodegenerative diseases. A common molecular hallmark of ALS and FTD is the pathological mislocalization and aggregation of ubiquitously expressed RNA-binding proteins (RBPs), such as TAR DNA-binding protein of 43 kDa (TDP-43) (Taylor et al., 2016). TDP-43 is normally predominantly nuclear, but in the degenerating brain regions of ALS and FTD patients, it is partially lost from the nucleus and instead aggregates in the cytoplasm of neurons and glial cells. RBP pathology is thought to cause neuronal dysfunction and neurodegeneration through a combination of nuclear loss-of-function and cytoplasmic gain-of-function mechanisms (Ling et al., 2013). Hence, it is essential to identify the molecular events that lead to this RBP misbehavior.

There is evidence that the combination of defective nuclear import and aberrant phase transitions of RBPs may give rise to the cytosolic RBP aggregates seen in *post mortem* brains of ALS and FTD patients (Dormann and Haass, 2011; Dormann et al., 2010; Lin et al., 2015; Molliex et al., 2015; Murakami et al., 2015; Patel et al., 2015; Zhang et al., 2019a). This hypothesis obtained strong support in recent years, when multiple groups studied the pathomechanism of the most frequent genetic cause of ALS and FTD, a large hexanucleotide repeat expansion in the *C9orf72* gene (DeJesus-Hernandez et al., 2011; Renton et al., 2011), and identified compelling links to both the nuclear transport machinery and liquid-liquid phase separation (LLPS) (Boeynaems et al., 2016a; Freibaum et al., 2015; Jovičić et al., 2015; Zhang et al., 2015). Healthy individuals have ≤11 repeats of a GGGGCC sequence in the first intron of the *C9orf72* gene, whereas patients with C9-ALS/FTD (the collective term for *C9orf72*-associated diseases) have hundreds to thousands of GGGGCC repeats

(Balendra and Isaacs, 2018). The expanded repeat sequence is bidirectionally transcribed into repeat RNA, which is then translated in every reading frame via repeat-associated non-AUG (RAN) translation, giving rise to five different dipeptide repeat proteins (DPRs; poly-GP, poly-GA, poly-GR, poly-PA, and poly-PR) (Ash et al., 2013; Mori et al., 2013). DPRs form predominantly cytoplasmic inclusions in brains of C9-ALS/FTD patients and are thought to cause proteotoxicity through a variety of different mechanisms (Balendra and Isaacs, 2018), although other toxicity mechanisms involving repeat RNAs and reduced *C9orf72* expression may also contribute to neurodegeneration in C9-ALS/FTD (Balendra and Isaacs, 2018; Swinnen et al., 2019; Webster et al., 2018). Among the different DPR species, arginine-rich (R-rich) DPRs were shown to be particularly toxic in both cell and animal models (Boeynaems et al., 2016a; Jovičić et al., 2015; Kramer et al., 2018; Kwon et al., 2014; Lee et al., 2016; Mizielinska et al., 2017; Tao et al., 2015; Wen et al., 2014; Zhang et al., 2018b). Although it is still debated whether neurodegeneration is linked to expression of specific DPRs (Mackenzie et al., 2013, 2015; Mann et al., 2013; Schludi et al., 2015), some studies have reported poly-GR to correlate with neurodegeneration and to be abundant in clinically related brain regions (motor cortex, frontal cortex, and spinal cord) (Gittings et al., 2020; Saberi et al., 2018; Sakae et al., 2018), supportive of a pathogenic role of R-rich DPRs.

Two major pathomechanisms appear to contribute to the toxicity of R-rich DPRs. First, independent genetic modifier screens in *Drosophila* and yeast revealed that poly-GR and poly-PR toxicity is strongly modulated by overexpression or reduction of different components of the nuclear transport machinery, including nucleoporins (Nups), nuclear transport receptors (NTRs), and regulators of the Ran system (Boeynaems et al., 2016a; Jovičić et al., 2015; Kramer et al., 2018; Lee et al., 2016). On the basis of these findings, it was proposed that R-rich DPRs may impair nucleocytoplasmic transport (NCT) and hence cause RBP mislocalization in C9-ALS/FTD (Boeynaems et al., 2016a, 2016b; Jovičić et al., 2015; Kim and Taylor, 2017; Zhang et al., 2016). However, the mechanistic link between R-rich DPRs and the NCT machinery remains elusive; that is, it is unclear whether poly-GR and poly-PR directly interact with components of the transport machinery (or rather indirectly via RBPs) and whether they indeed cause impaired nuclear import of C9-ALS/FTD-linked RBPs, such as TDP-43. Second, several proteomic studies have shown that R-rich DPRs interact with numerous intrinsically disordered proteins (IDPs) with low-complexity domains (LCDs) (Boeynaems et al., 2017; Lee et al., 2016; Lin et al., 2016). This interaction can alter LLPS of various IDPs, as demonstrated for NPM1/B23, hnRNP-A1, TIA-1 (Lee et al., 2016; White et al., 2019), and the LCD of FUS (Boeynaems et al., 2017). In line with these findings, cellular expression of or incubation of cells with short R-rich DPRs (GR_{50}, PR_{50}, or PR_{23}) disturbs the dynamics of several membrane-less organelles, including nucleoli, stress granules (SGs), nuclear speckles, and Cajal bodies (Lee et al., 2016; White et al., 2019). Whether phase separation of RBPs that aggregate in C9-ALS/FTD patients, such as TDP-43 (Murray et al., 2011; Simón-Sánchez et al., 2012; Stewart et al., 2012), is affected by poly-GR and poly-PR has so far not been examined.

We and others have recently shown that nuclear import receptors (importins) have a dual function and not only mediate nuclear import of nuclear localization sequence (NLS)-containing cargo proteins but also "chaperone" aggregation-prone RBPs, such as FUS, TDP-43, hnRNP-A1, and other hnRNPs linked to the ALS-FTD spectrum (Guo et al., 2018; Hofweber et al., 2018; Qamar et al., 2018; Yoshizawa et al., 2018). Several importins are known to bind to highly positively charged arginine- or lysine-rich NLSs. Thus, importins might directly bind to and chaperone the highly basic and R-rich DPR species poly-GR and poly-PR.

Here, we demonstrate that several importins, but not CRM1/Exportin-1, directly bind to R-rich DPRs and that this interaction can affect the biophysical properties of importins. Poly-GR and poly-PR peptides in molar excess reduce the solubility of several importins *in vitro* and in cytosol and cause importin condensation. Poly-GR, but not poly-PR, impairs nuclear import of a TDP-43 import reporter and of other classical NLS (cNLS)-containing model cargoes in intact cells. This import defect may act synergistically with aberrant phase separation of TDP-43 elicited by poly-GR and poly-PR. Interestingly, we find that increasing the concentration of importins can shield R-rich DPRs and thereby suppress their pathological aggregation with TDP-43 and RNA *in vitro* and under physiological conditions. This finding raises the possibility that a decrease in the endogenous concentration of importins, which may arise during physiological aging (Mertens et al., 2015; Nishimura et al., 2010; Pujol et al., 2002), could contribute to the pathogenesis of C9-ALS/FTD, and suggests that importins are promising therapeutic targets.

RESULTS

Importins Directly Bind to R-Rich DRPs

Several studies have identified NTRs as potential interactors of R-rich DPRs in proteomic approaches using total cell lysates (Boeynaems et al., 2017; Hayes et al., 2020; Lee et al., 2016). As NTRs continuously shuttle between the nucleus and cytosol, they could encounter DPRs in both compartments. In patients, however, DPRs are mostly found in the cytoplasm and less frequently in the nucleus (Ash et al., 2013; Gendron et al., 2013; Mackenzie et al., 2015; Mori et al., 2013), hence the interaction is more likely to occur in the cytosol. To investigate whether NTRs can interact with DPRs in the cytoplasm, we prepared cytosol from HeLa cells and incubated it with biotinylated DPR peptides as bait in a pull-down (PD) assay using physiological buffer conditions. Indeed, several NTRs bound to R-rich DPRs (GR_{25}, PR_{25}) but not to the non-charged control DPR GP_{25}. Imp7, Impβ, and Impα3 were bound equally to both poly-GR and poly-PR, while TNPO1 and TNPO3 bound preferentially to poly-GR (Figure 1A). Binding of the export receptor CRM1 to R-rich DPRs could not be detected, likely because its concentration in HeLa cytosol was too low (data not shown).

Although these findings confirm importins as physiological interactors of R-rich DPRs, it is still unclear whether this interaction is mediated by direct binding or conveyed indirectly (e.g., by RBPs or other cargoes). As NTRs are negatively charged (Cansizoglu et al., 2007; Lott and Cingolani, 2011) and hence could directly bind to positively charged R-rich DPRs, we investigated whether our biotinylated DPR peptides directly interact with purified, recombinant NTRs in *in vitro* PD assays. After stringent washing, we detected prominent binding of TNPO1 and Impβ

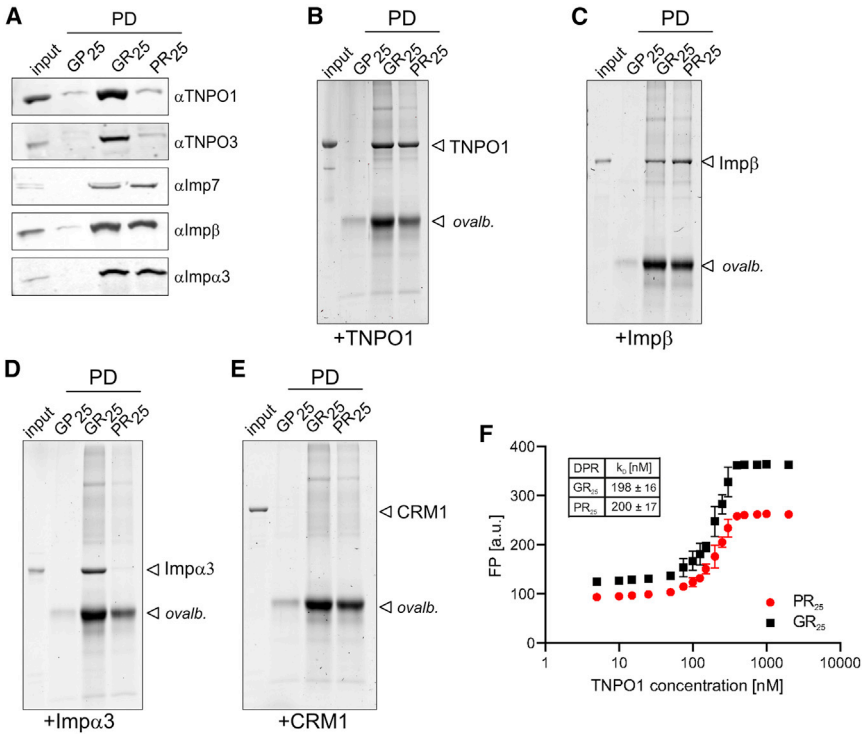

Figure 1. Importins Bind Directly to Arginine-Rich Dipeptide Repeat Proteins (DPRs)

(A) Western blot showing binding of endogenous importins from HeLa cytosol to immobilized, biotinylated GR_{25} and PR_{25}, but not GP_{25}, in a pull-down (PD).

(B–E) Direct binding of R-rich DPRs to the importins TNPO1 (B), Impβ (C), Impα3 (D), but not CRM1 (E) in pull-downs using biotinylated GR_{25}, PR_{25}, and GP_{25} (bait) and purified importins (prey) visualized by Sypro-Ruby staining. Input represents 5% of the importin used in the PD. Ovalbumin (ovalb.) was used to prevent unspecific binding to the beads.

(F) Fluorescence polarization measurements of fluorescein isothiocyanate (FITC)-labeled GR_{25} (black) or PR_{25} (red) with increasing concentrations of TNPO1. Table shows calculated k_D values assuming a 1:1 complex formation representing the mean of three independent experiments performed in technical triplicate ± SEM of the fit.

See also Figure S1.

to both poly-GR and poly-PR, but not poly-GP (Figures 1B and 1C). Moreover, recombinant Imp5, Imp7, Imp9, and TNPO3 strongly bound to R-rich DPRs but not poly-GP (Figures S1A–S1D). We also tested direct binding of R-rich DPRs to Impα. We observed direct binding of two Impα isoforms, Impα3 (Figure 1D) and Impα1 (Figure S1E), preferentially to poly-GR. In contrast, no binding of the purified export receptor CRM1 to the tested DPRs could be detected (Figure 1E).

To further characterize the interaction of poly-GR and poly-PR with importins, we measured the binding affinity of GR_{25} or PR_{25} to TNPO1, an importin involved in nuclear import of many RBPs, using fluorescence polarization (Moerke, 2009). Here, both R-rich DPRs displayed similar affinity binding to TNPO1 ($k_D \sim$ 200 nM; Figure 1F). Together, our data demonstrate that several importins, but not the exportin CRM1, directly bind to the R-rich DPRs poly-GR and poly-PR with high affinity.

R-Rich DPRs Cause the Formation of Solid-like Importin Condensates

We next characterized the consequences of the DPR-importin interaction at the molecular level. R-rich DPRs were shown to promote aberrant phase separation of RBPs and to change the biophysical properties of their interacting proteins (Boeynaems et al., 2017; Lee et al., 2016; Shi et al., 2017), hence we tested whether increasing concentrations of poly-GR or poly-PR affect the solubility of Impα/β, the best characterized import receptor for cNLS-containing cargo proteins. In a sedimentation assay, both Impβ and its adaptor protein Impα are detected in the supernatant (S) in the absence of R-rich DPRs, reflecting their high solubility (Figures S2A and S2C). However, upon addition of increasing concentrations of either GR_{25} (Figures S2A and S2B) or PR_{25} (Figures S2C and S2D), both Impα and Impβ shifted progressively into the pellet fraction (P), indicating reduced solubility in the presence of high GR or PR concentrations. Notably, Impα appeared more sensitive than Impβ to an excess of R-rich DPRs, as higher concentrations of GR_{25} or PR_{25} peptides were required for efficient precipitation of Impβ (Figures S2A–S2D). To determine whether this effect is specific for R-rich DPRs, we compared the sedimentation behavior of Impα/β in the presence of a 10-fold excess of GR_{25}, PR_{25}, or GP_{25} (Figures 2A and 2B). Compared with poly-GR, poly-PR was slightly less efficient in precipitating Impα but showed a similar effect toward Impβ. The non-charged DPR species poly-GP had no effect on the solubility of either Impα or Impβ, indicating the importance of arginine in this process. Interestingly, a shorter GR peptide (GR_{10}) had only a minor effect on the solubility of Impα and no effect on Impβ, suggesting that a certain minimum number of GR repeats is required for efficient precipitation of Impα/β. Longer GR repeats, which are likely found in C9-ALS/FTD patients, could be even more potent in reducing Impα/β solubility and in promoting phase separation in general.

To address whether R-rich DPRs also reduce the solubility of other NTRs, we analyzed TNPO1, Impβ (in the absence of Impα), Impα (in absence of Impβ), and CRM1 in the sedimentation assay. Among these NTRs, Impα and TNPO1 were efficiently precipitated by 10-fold molar excess of GR_{25} and PR_{25}, but not by poly-GP. A shorter GR peptide (GR_{10}) showed no or only a minor effect, emphasizing the importance of the repeat length (Figures 2C and 2D). In contrast, Impβ and CRM1 remained mainly soluble in presence of either poly-GR or poly-PR. Titration of GR_{25} and PR_{25} showed enhanced susceptibility of both TNPO1 (Figures S2E–S2H) and Impα alone (Figures S2I–S2K) to already small molar excess (5×) of R-rich peptides, whereas Impβ and CRM1 exhibited only partial or no precipitation even at extremely high concentrations of poly-GR and poly-PR (Figures S2E–S2H).

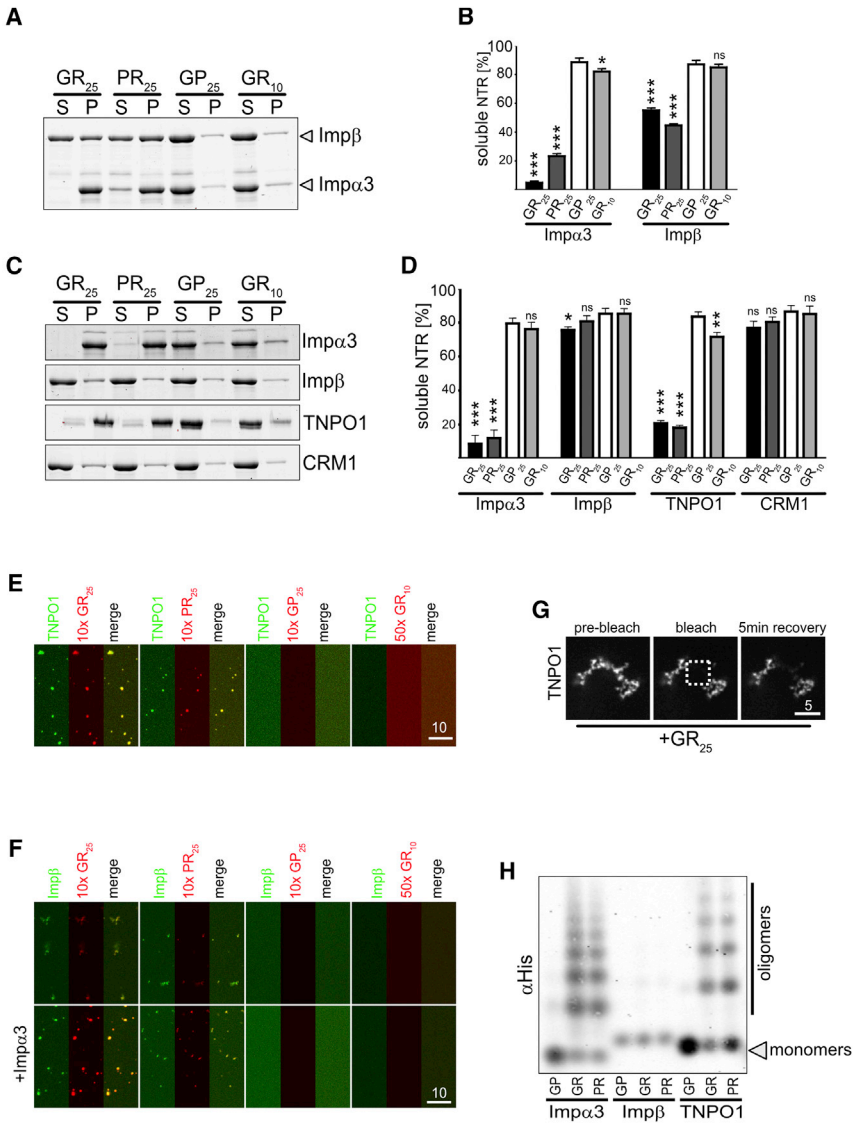

Figure 2. Poly-GR and Poly-PR Reduce the Solubility of Importins and Cause Their Condensation and Oligomerization

(A) Sedimentation assay to measure precipitation of recombinant His-Impα3/His-S-Impβ by 10-fold molar excess of TMR-GR_{25}, TMR-PR_{25}, TMR-GP_{25}, or TMR-GR_{10} visualized by Sypro-Ruby staining.

(B) Percentage of the respective importin being soluble shown as mean of three independent experiments ± SEM; *$p < 0.0322$ and ***$p < 0.0002$ by one-way ANOVA with Dunnett's multiple-comparison test to GP_{25}.

(C) Sedimentation assay to quantify precipitation of recombinant His-Impα3, His-S-Impβ, His-TNPO1, or CRM1 in the presence of 10-fold molar excess of either TMR-GR_{25}, TMR-PR_{25}, or TMR-GP_{25} visualized by Sypro-Ruby staining.

(D) Percentage of the respective NTR being soluble as the mean of three independent experiments ± SEM; *$p < 0.0322$, **$p < 0.021$, and ***$p < 0.0002$ by one-way ANOVA with Dunnett's multiple-comparison test to GP_{25}.

(E) GFP-TNPO1 forms condensates in the presence of a 10-fold molar excess of TMR-labeled GR_{25} and PR_{25}, but not with TMR-GP_{25} or a 50-fold excess of TMR-GR_{10}. Scale bar, 10 μm.

(F) Condensate formation of GFP-Impβ in the presence of a 10-fold molar excess of TMR-labeled GR_{25} or TMR-PR_{25}, but not TMR-GP_{25} or a 50-fold excess of TMR-GR_{10}, is enhanced by equimolar amounts of Impα3 (unlabeled). Scale bar, 10 μm.

(G) FRAP demonstrating reduced mobility of GFP-TNPO1 condensates induced by 10-fold molar excess of TMR-GR_{25}. Scale bar, 5 μm.

(H) Anti-His western blot demonstrating oligomer formation of His-Impα3 and His-TNPO1, but not His-S-Impβ, by 10-fold molar excess of TMR-GR_{25} and TMR-PR_{25} shown by SDD-AGE.

See also Figure S2.

We also observed altered biophysical properties of TNPO1 in the presence of excess poly-GR and poly-PR using fluorescence microscopy. Upon mixing of GFP-TNPO1 with a 10-fold molar excess of tetramethylrhodamine (TMR)-labeled GR_{25} or PR_{25} peptides, small condensates containing both GFP-TNPO1 and TMR-GR_{25} or TMR-PR_{25} were observed using confocal microscopy (Figure 2E). TMR-GP_{25} or a shorter GR peptide (TMR-GR_{10}), even at high molar excess (50×), caused no TNPO1 condensation (Figure 2E). In contrast to TNPO1 and in line with our sedimentation analysis, GFP-Impβ condensed more efficiently with R-rich DPRs in the presence of Impα (Figure 2F). To characterize GR- and PR-induced NTR condensates further, we first analyzed the dynamicity of poly-GR-induced TNPO1 condensates using fluorescence recovery after photobleaching (FRAP). No recovery of the bleached area in GFP-TNPO1 condensates could be detected within 5 min after the bleach, indicating low internal mobility (Figure 2G). Moreover, semi-denaturing detergent agarose gel electrophoresis (SDD-AGE) showed that condensates of TNPO1 and Impα3 formed by 10-fold molar excess of poly-GR and poly-PR, but not poly-GP, represent SDS-resistant oligomers of TNPO1 and Impα3 (Figure 2H), suggesting crosslinking of individual TNPO1 and Impα3 molecules by R-rich DPRs. In line with our sedimentation and microscopy analysis, no oligomers could be detected for Impβ in presence of R-rich DPRs (Figure 2H). Analysis of TNPO1 experimental radial density distributions (P[r]) in absence or presence of up to 2-fold molar excess of GR_{25} or PR_{25} by small-angle X-ray scattering (SAXS) in solution showed no change, indicating that TNPO1 molecules that remained in solution under these conditions were monomeric (Figures S2L and S2M). Higher excess of DPRs with TNPO1 resulted in precipitation of TNPO1 and hence prohibited SAXS analysis.

Taken together, our data demonstrate that R-rich DPRs in a concentration- and repeat length-dependent manner affect the biophysical properties of importins and induce their precipitation and condensate formation. Interestingly, import receptors differ

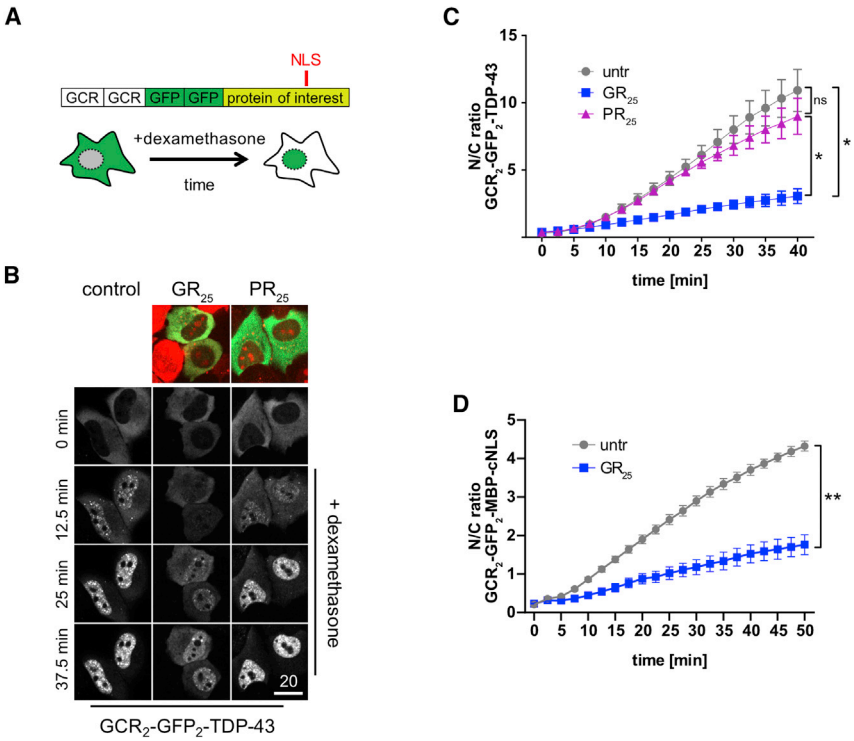

Figure 3. Poly-GR Interferes with Nuclear Import of TDP-43 and Other cNLS-Containing Cargoes

(A) Experimental design of the hormone-inducible nuclear import reporter assay. GCR_2-GFP_2 is fused to a protein of interest carrying a NLS. Upon cellular expression, the reporter remains cytoplasmic but is actively imported into the nucleus over time upon addition of the steroid hormone dexamethasone.

(B) Delayed import of GCR_2-GFP_2-TDP-43 by GR_{25}, but not PR_{25}, by live cell imaging compared with untreated cells (control). Scale bar, 20 μm. Uptake of TMR-labeled DPR peptides (red) by GCR_2-GFP_2-TDP-43-expressing cells (green) before dexamethasone addition was verified by confocal imaging (top row).

(C) Nuclear/cytoplasmic (N/C) ratio of fluorescence intensities of GCR_2-GFP_2-TDP-43 import over time shown as mean of three independent experiments (20–51 cells each) ± SEM. Statistical significance was calculated by repeated-measures (RM) one-way ANOVA for the area under the curve with Tukey's multiple comparison test (*$p < 0.0332$).

(D) Nuclear/cytoplasmic (N/C) ratio of fluorescence intensities of GCR_2-GFP_2-MBP-cNLS import over time in either untreated cells (untr) or cells pre-incubated TMR-GR_{25} (GR_{25}) as mean of three independent experiments (19–69 cells each) ± SEM. Statistical significance was calculated by comparing the area under the curve by unpaired t test (**$p < 0.0021$).

See also Figure S3.

in their susceptibility toward R-rich DPRs, with TNPO1, Impα, and Impα/β being more susceptible than Impβ alone.

Poly-GR Impairs Nuclear Import of a TDP-43 Reporter and Other cNLS-Containing Model Cargoes

Nuclear depletion and cytoplasmic aggregation of TDP-43 is a pathological hallmark of C9-ALS/FTD (Murray et al., 2011; Simón-Sánchez et al., 2012; Stewart et al., 2012). TDP-43 contains a bipartite cNLS and is imported by Impα/β (Nishimura et al., 2010; Winton et al., 2008). Considering the reduced solubility of Impα/β in presence of R-rich DPRs (Figures 2A and 2B), we speculated that nuclear import of TDP-43 could be impaired by R-rich DPRs. Indeed, it has been previously suggested that reduced nuclear import of TDP-43 caused by DPRs could underlie the observed TDP-43 pathology (Khosravi et al., 2017; Solomon et al., 2018), but this hypothesis has not been addressed in *bona fide* nuclear import assays. To analyze the impact of R-rich DPRs on nuclear import of TDP-43 in intact cells, we made use of a hormone-inducible import system adapted from (Love et al., 1998). Here, the protein of interest is fused to two GFP moieties for visualization (GFP_2) and two hormone binding domains of the glucocorticoid receptor (GCR_2). The GCR domains retain the reporter in the cytoplasm, but upon addition of a steroid hormone (dexamethasone), it is released and subsequently imported into the nucleus, dependent on the NLS in the protein of interest (Figure 3A). Indeed, a GCR_2-GFP_2-TDP-43 reporter transiently expressed in HeLa cells localizes mainly to the cytoplasm but accumulates within minutes in the nucleus upon addition of dexamethasone, as visualized by live cell imaging (Figure 3B, control). To follow its nuclear import in the presence of poly-GR or poly-PR, we added 10 μM TMR-labeled GR_{25} or PR_{25} peptides to the culture medium, as they are known to enter cells because of their strong positive charge (Kwon et al., 2014) (Figure 3B, top row). Interestingly, after pre-incubation of cells with GR_{25} for 2 h, nuclear import of the TDP-43 reporter was strongly decelerated in GR-positive cells (Figure 3B; see Figure 3C for quantification of N/C ratio over time). In contrast, incubation of cells with the PR_{25} peptide had only a minor effect on TDP-43 import, indicating that the TDP-43 import defect was specifically induced by poly-GR. The observed import defect was not dependent on the presence of the LCD in TDP-43, as a TDP-43 reporter lacking this domain (GCR_2-GFP_2-TDP-43 ΔLCD) still exhibited reduced nuclear import in presence of poly-GR (Figures S3A and S3B). Nuclear transport defects have previously been attributed to the presence of SGs, which contain essential nuclear transport factors (Zhang et al., 2018a). Hence, we examined cells expressing GCR_2-GFP_2-TDP-43 after exposure to TMR-labeled DPRs for the presence of SGs by co-staining for the SG marker TIA-1. However, we could not detect enhanced TIA-1-positive foci in DPR-positive cells expressing the TDP-43 reporter (Figure S3C). Thus, poly-GR interferes with efficient nuclear import of TDP-43 independently of the presence of SGs.

To investigate whether poly-GR affects Impα/β-mediated import in general, we next analyzed cells expressing GCR_2-GFP_2-MBP-cNLS, a reporter with a similar size as GCR_2-GFP_2-TDP-43. Nuclear import of the MBP-cNLS reporter was also significantly reduced by poly-GR (Figure 3D), suggesting a general import defect for cNLS-bearing cargoes caused by poly-GR. Also, a smaller reporter containing only the SV40 cNLS

(GCR_2-GFP_2-cNLS) showed reduced nuclear import in presence of poly-GR (Figure S3D). Notably, diffusion of the reporter in absence of any NLS (GCR_2-GFP_2) into the nucleus was only mildly affected by poly-GR (Figure S3D), indicating that poly-GR predominantly interferes with the functionality of Impα/β. Moreover, the mobility of the GCR_2-GFP_2 reporter in the cytoplasm was unchanged by presence of poly-GR as evidenced by FRAP, indicating unchanged solubility of our reporter (Figure S3D). Nevertheless, we cannot fully exclude additional effects of poly-GR on the nuclear pore and/or on the GCR-reporter system.

Taken together, our data support the idea that poly-GR impairs nuclear import of TDP-43 and potentially other cargoes requiring active, NLS- and importin-dependent import into the nucleus.

R-Rich DPRs Promote Phase Separation and Insolubility of TDP-43

R-rich DPRs have previously been shown to promote LLPS of diverse RBPs, such as TIA-1, NPM1/B23 and hnRNPA1 (Lee et al., 2016; White et al., 2019). Whether poly-GR and poly-PR also promote phase transition of TDP-43 has not been examined yet. TDP-43 is a highly aggregation-prone RBP, but can be purified as soluble protein via fusion to a cleavable MBP-His_6 solubility tag (TDP-43-*Tev*-MBP-His_6; Wang et al., 2018) allowing for controlled induction of phase separation by cleavage with Tev protease. To visualize TDP-43 condensates using fluorescence microscopy, we spiked in His_6-MBP-*Tev*-TDP-43-GFP at substoichiometric concentrations. At low TDP-43 concentrations (2 μM TDP-43/TDP-43-GFP), no visible condensates were formed 30–60 min after Tev protease-mediated cleavage of the MBP solubility tag (Figure 4A). However, the presence of TMR-labeled R-rich DPRs led to the formation of condensates containing both TDP-43 and poly-GR or poly-PR, respectively, while poly-GP had no effect (Figure 4A).

To determine the effect of poly-GR and poly-PR on condensation of TDP-43 more quantitatively, we evaluated the sedimentation of TDP-43 in the absence or presence of DPRs in a sedimentation assay. We chose experimental conditions (200 mM NaCl) that resulted in only partial sedimentation of cleaved TDP-43 (~50% solubility; Figures 4B and 4C), allowing us to detect a promoting effect by poly-GR/PR. Already equimolar concentrations of both TMR-GR_{25} and TMR-PR_{25}, but not TMR-GP_{25}, significantly promoted the sedimentation of TDP-43 into the pellet fraction (Figures 4B and 4C). To examine whether enhanced insolubility of TDP-43 could also be observed in intact cells, we incubated HeLa cells with or without GR_{25} or PR_{25} peptides and subsequently analyzed TDP-43 solubility in RIPA buffer by western blot. Interestingly, incubation of cells for only 2 h with either GR_{25} or PR_{25} resulted in a significant increase of TDP-43 in the insoluble (pellet) fraction (Figures 4D–4F).

Collectively, our data demonstrate that R-rich DPRs promote phase separation and reduce the solubility of TDP-43, both *in vitro* and in cells.

Increasing Importin Concentrations Can Shield R-Rich DPRs and Suppress Poly-GR-Induced Phase Separation of RBPs or RNA *In Vitro*

Several Impβ-type importins have been found to execute a chaperoning function toward aggregation-prone proteins, including RBPs, FG-rich Nups, ribosomal proteins, and histones (Guo et al., 2018; Hofweber et al., 2018; Jäkel et al., 2002; Milles et al., 2013; Qamar et al., 2018; Yoshizawa et al., 2018). Having observed the direct interaction of R-rich DPRs with Impβ-type importins (Figure 1), we wondered whether importins could also shield R-rich DPRs and thus prevent them from promoting aberrant phase transitions of RBPs. To address this question, we first evaluated the formation of poly-GR- or poly-PR-induced TDP-43 condensates in the absence or presence of different NTRs *in vitro* using fluorescence microscopy. Indeed, equimolar concentrations of TNPO1, Impβ, or Impα/β could suppress the GR- or PR-induced formation of TDP-43 condensates, while CRM1 or Impα3 alone had no effect (Figures 5A and S4A). To confirm that TNPO1 and Impβ suppress TDP-43/GR_{25}-phase transition by shielding poly-GR and not TDP-43 itself, we tested whether these importins were able to suppress phase separation of TDP-43 alone. To this end, we examined TDP-43-*Tev*-MBP/MBP-*Tev*-TDP-43-GFP condensates (5 μM) in the presence or absence of different NTRs. Only Impα/β, the cognate import receptor for TDP-43, could efficiently suppress phase separation of TDP-43, as described previously (Guo et al., 2018), whereas TNPO1, Impβ or CRM1 were unable to abolish condensate formation of TDP-43 (Figure S4B). These findings confirm that neither TNPO1 nor Impβ alone acts on TDP-43 directly but suppresses GR-induced phase transition of TDP-43 by binding to poly-GR.

To quantitatively validate that importins are able to suppress poly-GR-mediated phase separation of TDP-43 by sequestering poly-GR, we performed a sedimentation assay. Addition of TNPO1, Impβ, or Impα/β prior to Tev protease cleavage efficiently reverted the poly-GR-enhanced sedimentation of TDP-43, while CRM1 showed only minor shielding activity (Figures 5B and 5C). In accordance with the microscopic condensate assay, GST-GR_{25} was completely soluble in the absence of TDP-43, but moved efficiently into the pellet fraction in the presence of cleaved TDP-43 (Figures 5D and 5E). Furthermore, the solubility of GST-GR_{25} in the presence of TDP-43 was completely rescued by addition of equimolar concentrations of TNPO1, Impβ, or Impα/β, whereas CRM1 was unable to rescue the TDP-43 induced precipitation of GST-GR_{25} (Figures 5D and 5E). GR-shielding activity of TNPO1 was also confirmed by turbidity assay in a time-sensitive manner. Here, TNPO1 effectively suppressed GR-mediated promotion of TDP-43 turbidity but did not affect the increase in TDP-43 turbidity in absence of GR after by Tev cleavage of the MBP tag (Figures S4C and S4D).

R-rich DPRs have also been shown to form condensates with polyanions, such as RNA (Boeynaems et al., 2017, 2019), and the interactions of poly-GR/PR with nucleic acids were proposed to have detrimental consequences on RNA- and DNA-based processes and cause heterochromatin abnormalities (Boeynaems et al., 2019; Lafarga et al., 2019; Zhang et al., 2019b). We therefore tested whether importins are also able to suppress the formation of poly-GR/RNA condensates. Indeed, equimolar concentrations of either TNPO1 or Impβ were able to suppress RNA-mediated condensation of poly-GR *in vitro* (Figure 5F). In contrast, poly-GR and

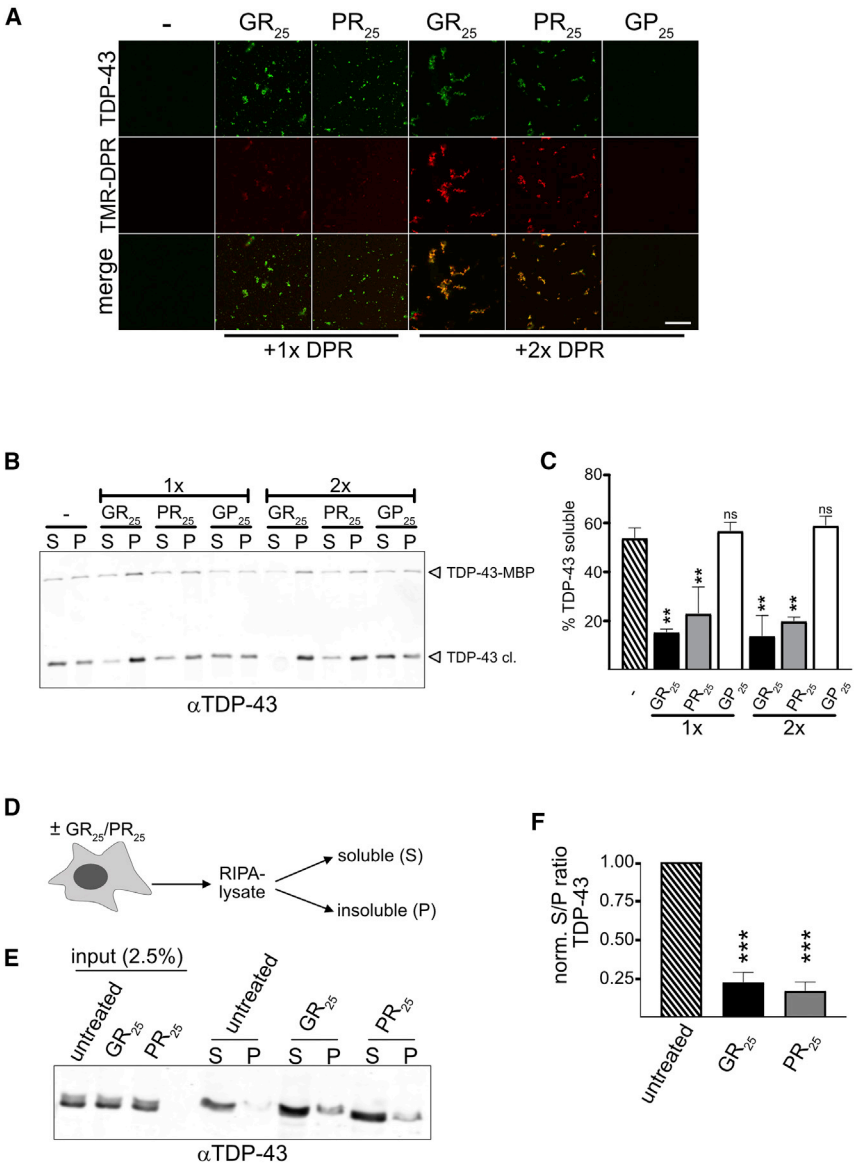

Figure 4. Poly-GR and Poly-PR Promote Phase Separation of TDP-43

(A) Condensate formation upon Tev cleavage of TDP-43-*Tev*-MBP/MBP-*Tev*-TDP-43-GFP in the absence (–) or presence of equimolar (1×) or two-fold (2×) molar excess of TMR-labeled DPRs. Scale bar, 20 μm.

(B) Anti-TDP-43 western blot showing that both TMR-GR_{25} and TMR-PR_{25} promote sedimentation of TDP-43 upon Tev cleavage of TDP-43-*Tev*-MBP more strongly than TMR-GP_{25}. Note that Tev cleavage of the MBP tag is not complete in all reactions but that uncleaved TDP-43-MBP mirrors the sedimentation behavior of cleaved TDP-43 (likely because of multimerization).

(C) Quantification of the amount of soluble, cleaved TDP-43 as mean of three independent experiments ± SEM; **p < 0.0021 by one-way ANOVA with Dunnett's multiple-comparison test to untreated (–).

(D) Experimental design to address RIPA-buffer solubility of endogenous TDP-43 upon incubation of intact cells with GR_{25}/PR_{25} peptides shown in (E).

(E) RIPA-soluble (S) and insoluble (P) fractions were analyzed using TDP-43 western blot (WB). Note that for visibility, the pellet fraction in the WB is overrepresented 4.5×.

(F) Normalized S/P ratio for TDP-43 after correction for overrepresentation of the pellet fraction as mean of three independent experiments ± SEM; **p < 0.0021 by one-way ANOVA with Dunnett's multiple-comparison test to untreated (–).

RNA still formed condensates in the presence of Impα3 or CRM1 (Figure 5F), consistent with our earlier observation with TDP-43.

In summary, several DPR-interacting importins of the Impβ family, but not Impα or the export receptor CRM1, are able to shield R-rich DPRs from binding to and enhancing phase separation of RBPs and RNA *in vitro*.

Increasing Importin Concentrations Can Suppress DPR-Induced TDP-43 Precipitation in the Cytosol

Having characterized the impact of R-rich DPRs on importins and TDP-43 using purified components *in vitro*, we sought to investigate whether R-rich DPRs can also induce precipitation of interacting importins and TDP-43 under more physiological conditions using HeLa cytosol instead of recombinant proteins in our sedimentation assay. Indeed, TNPO1, Impα3, Impβ, and TDP-43 were efficiently precipitated from HeLa cytosol by addition of poly-GR and poly-PR, but not poly-GP, in a concentration-dependent manner (Figures 6A and 6B), despite the presence of other cellular poly-GR/PR interactors. Importantly, this effect did not affect all cytosolic proteins, as GAPDH was not precipitated even by the highest GR/PR concentrations (Figures 6A and 6B).

Next, we tested whether increased concentration of importins can also suppress poly-GR-mediated precipitation of TDP-43 from HeLa cytosol. As shown in Figure 6C, addition of equimolar concentrations of TNPO1, Impβ, or Impα/β, but not CRM1, efficiently suppressed GR-induced precipitation of cytosolic TDP-43 (Figures 6C and 6D).

Taken together, we find that diverse importins suppress poly-GR-induced condensation of TDP-43 or RNA, suggesting that importins could have a broadly protective effect by buffering pathological interactions of poly-GR with other macromolecules, including disease-linked RBPs, nucleic acids, and potentially other interactors reported for R-rich DPRs (Boeynaems et al., 2017; Choi et al., 2019; Fumagalli et al., 2019; Hartmann et al., 2018; Lafarga et al., 2019; Lee et al., 2016; Moens et al., 2019; Zhang et al., 2019b).

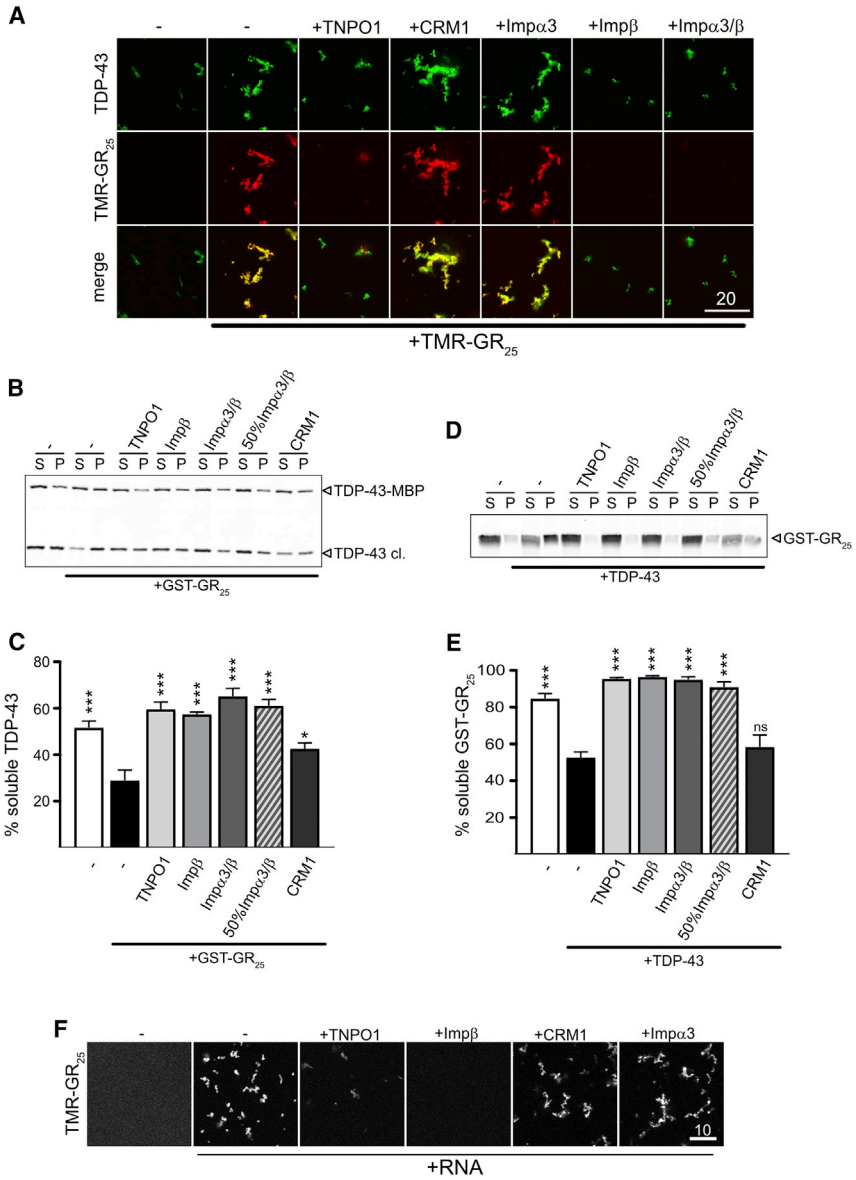

Figure 5. Importins Shield R-Rich DPRs and Suppress Condensate Formation with TDP-43 or RNA

(A) Equimolar concentrations of TNPO1, Impβ, or Impα3/β, but not CRM1 or Impα3 alone, prevent poly-GR-induced phase separation of TDP-43. Scale bar, 20 μm.

(B) Anti-TDP-43 western blot showing sedimentation of TDP-43 upon Tev cleavage in the presence of GST-GR_{25} and the absence or presence of various NTRs. Note that Tev-mediated cleavage of the MBP tag is not complete in all reactions but that uncleaved TDP-43-MBP mirrors the sedimentation behavior of cleaved TDP-43 (likely because of multimerization).

(C) Percentage of soluble, cleaved TDP-43 as mean of three independent experiments ± SEM; ***p < 0.0002 and *p < 0.0332 by one-way ANOVA with Dunnett's multiple-comparison test to untreated (–) in the absence of GST-GR_{25}.

(D) Anti-GST western blot showing sedimentation of GST-GR_{25} in the absence or presence of TDP-43 and various NTRs.

(E) Percentage of soluble GST-GR_{25} shown as mean of three independent experiments ± SEM; ***p < 0.0002 by one-way ANOVA with Dunnett's multiple-comparison test to untreated (–) in the absence of TDP-43.

(F) Condensation of TMR-GR_{25} by RNA is suppressed by equimolar concentrations of TNPO1 or Impβ, but not CRM1 or Impα3. Scale bar, 10 μm. See also Figure S4.

DISCUSSION

R-Rich DPRs Directly Bind to Importins and Mediate Importin Condensation in a Concentration- and Repeat Length-Dependent Manner

Importins have been identified as strong genetic modifiers of poly-GR- and poly-PR-mediated cellular toxicity in several independent studies in *Drosophila* and yeast (Boeynaems et al., 2016a; Jovičić et al., 2015; Kramer et al., 2018; Lee et al., 2016). Additionally, several proteomic studies have previously identified importins as cellular interactors of poly-GR or poly-PR (Boeynaems et al., 2016a; Lee et al., 2016; Lin et al., 2016). So far, it has been unclear whether this interaction is direct or indirect (e.g., mediated by RBPs bound to importins), and the underlying mechanism for modification of cellular toxicity by importins has not been addressed. Using *in vitro* PDs with purified recombinant proteins, we now demonstrate that R-rich DPRs bind directly to a number of different importins, likely by charge-charge-driven interactions, but not to the export receptor CRM1. Binding of R-rich DPRs to TNPO1 was determined to be of relatively high affinity (k_D in the low nanomolar range), suggesting this interaction is likely to happen in cells. Our data are in line with recent work showing direct binding of poly-PR and poly-GR to Impβ *in vitro* using FRET sensors and bead Halo assays (Hayes et al., 2019), but no other NTRs were analyzed in this study. Here, we find that multiple importins have the capacity to directly bind to R-rich DPRs.

Interestingly, the consequences of the direct importin-DPR interaction strongly depend on the molecular ratio of DPRs to importins. In excess, short R-rich DPR peptides (GR_{25} and PR_{25}) reduce the solubility of several importins in a concentration-dependent manner, particularly Impα, Impα/β, and TNPO1. Longer DPR repeats, as they are likely found in C9-ALS/FTD patients, could have the same effect at even reduced concentrations. Notably, import receptors differ in their sensitivity toward poly-GR or poly-PR. Among the importins analyzed, TNPO1 and Impα appear particularly susceptible to precipitation by R-rich DPRs. DPR-driven precipitation of Impα also promotes insolubility of

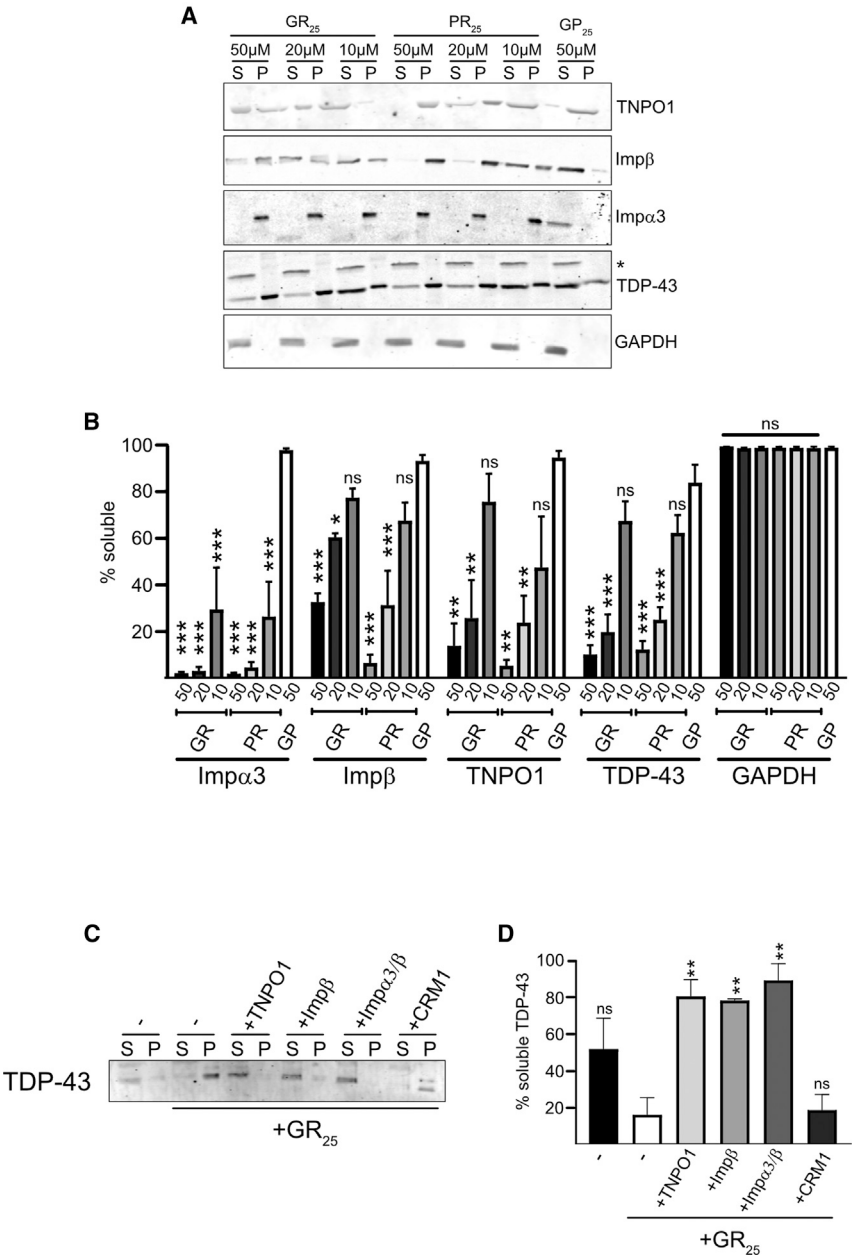

Figure 6. Importins Can Suppress Poly-GR-Induced TDP-43 Precipitation from Cytosol

(A) Western blot demonstrating that importins and TDP-43, but not GAPDH, are precipitated by poly-GR and poly-PR, but not poly-GP, in a concentration-dependent manner from HeLa cytosol; asterisk marks an unspecific band.

(B) Percentage of soluble protein shown as mean of three or four independent experiments ± SEM; **p < 0.0021 and ***p < 0.0002 by one-way ANOVA with Dunnett's multiple-comparison test to GP_{25}.

(C) Anti TDP-43 western blot demonstrating poly-GR-induced precipitation of TDP-43 from HeLa cytosol can be prevented by addition of TNPO1, Impβ, or Impα/β, but not by CRM1.

(D) Percentage of soluble TDP-43 in the presence of poly-GR and NTRs as mean of three independent experiments ± SEM; **p < 0.0021 by one-way ANOVA with Dunnett's multiple comparison test to TDP-43/GR_{25}.

Impβ, as Impβ was precipitated more strongly by R-rich DPRs in the presence of Impα than in its absence. For all importins tested, poly-GP had no effect on solubility, underscoring the role of arginine in the interaction and precipitation of import receptors. Poly-GR/PR-induced phase separation has recently been reported to occur for several RBPs with intrinsically disordered LCDs (Boeynaems et al., 2017; Lee et al., 2016; White et al., 2019). NTRs, however, are overall predominantly structured proteins (Christie et al., 2016) and have been suggested to have a very low intrinsic aggregation propensity (Frey et al., 2018). Strikingly, our data show that molar excess of GR_{25} and PR_{25} changes the biophysical properties of specific NTRs, most notably Impα/β and TNPO1, and causes their precipitation and condensation even at stringent salt concentrations (200 mM NaCl). Currently, it is unclear whether such DPR levels are reached in patients. However, intriguingly, a shorter GR peptide (GR_{10}) failed to precipitate Impα/β or TNPO1. This repeat length dependence suggests that longer DPRs might exert similar effects already at reduced concentrations. Even 25mers of R-rich DPRs cause oligomerization of TNPO1 and Impα, as demonstrated by SDD-AGE, hence increased repeat length, as found in patients, might even be more potent in crosslinking several importin molecules at once. Importantly, precipitation of importins by R-rich DPRs also happens under physiological conditions (i.e., in the presence of numerous other cellular poly-GR/PR interactors), as seen in precipitation assays with HeLa cytosol. In line with our findings, precipitation of importins by R-rich DPRs from cell lysates has been reported previously (Boeynaems et al., 2017; Hayes et al., 2019). Importantly, however, we now demonstrate that this precipitation might be due to a direct effect of R-rich DPRs on importin solubility that can be reconstituted *in vitro* and could happen in the absence of aggregation-prone RBP cargoes bound to importins.

The DPR-induced precipitation of importins observed in our *in vitro* assays raises the question whether R-rich DPRs could trigger insolubility and aggregation of importins in C9-ALS/FTD patients. Interestingly, some Impα isoforms were found to colocalize with cytosolic poly-GR granules in a poly-GR_{200} mouse model (Cook et al., 2020). Also, Impα3 (KPNA4) pathology (i.e., nuclear depletion and cytoplasmic mislocalization of Impα3) has been reported in C9-ALS/FTD *post mortem* brain (Solomon

et al., 2018). Although this effect could be linked to DPR (in particular poly-GR) expression in the absence of any major NPC defects, it was also observed in absence of DPR pathology and thus proposed to be caused by TDP-43 pathology. However, reduced solubility of Impα induced by poly-GR, as observed in our *in vitro* assay, could underlie the cytoplasmic mislocalization and reduced solubility of Impα observed in C9-ALS/FTD patients (Solomon et al., 2018) and in poly-GR_{200} mice (Cook et al., 2020) and could result in reduced availability of Impα for nuclear import. Whether solubility of other importins, such as Impβ and TNPO1, is affected in C9-ALS/FTD patients remains elusive. Absence of Impβ pathology in C9-ALS was reported recently (Saberi et al., 2018), but a subtler insolubility of Impβ or other import receptors in affected brain regions cannot be excluded and remains to be addressed biochemically.

Poly-GR Interferes with cNLS-Mediated Nuclear Import, Including Import of TDP-43

Conflicting data exist as to whether R-rich DPRs impair NCT and hence could directly contribute to mislocalization of RBPs, such as TDP-43, in C9-ALS/FTD. Several studies have reported mislocalization of NCT factors, such as Ran, RanGAP, or Nups (Cook et al., 2020; Freibaum et al., 2015; Odeh and Shorter, 2020; Zhang et al., 2015, 2016); nuclear accumulation of mRNA (Freibaum et al., 2015; Shi et al., 2017); or genetic modulation of poly-GR/PR toxicity by NCT factors (Boeynaems et al., 2016a; Jovičić et al., 2015; Kramer et al., 2018; Lee et al., 2016) but have not addressed NCT defects explicitly by NCT assays. Recently, defective import of Impβ and TNPO1 model cargoes has been reported to occur with high DPR concentrations (50–100 μM of 10- or 20mers) using semi-permeabilized cells (Hayes et al., 2020). Some studies have used shuttling reporters (fluorescent protein fused to both an NLS and a nuclear export signal) and reported reduced import in C9-ALS/FTD patient-derived induced pluripotent stem cells (iPSCs) (Zhang et al., 2015) and in HeLa cells upon incubation with poly-PR peptides (Shi et al., 2017). In contrast, no import defect for a similar shuttling reporter was detected upon either cellular DPR expression or upon incubation of cells with GR_{20} or PR_{20} peptides, unless cells exhibited SGs (Vanneste et al., 2019). The latter finding is consistent with a previous report suggesting that SGs sequester various NCT factors and thus impair NCT (Zhang et al., 2018a). Whether SGs were elicited in the earlier studies reporting NCT defects in C9-ALS/FTD (Shi et al., 2017; Zhang et al., 2015) is not known.

Remarkably, it has not yet been addressed whether R-rich DPRs impair nuclear import of disease-linked RBPs, in particular TDP-43, the major aggregating protein in C9-ALS/FTD. Here, we have used a hormone-induced nuclear import reporter assay to demonstrate that TDP-43 nuclear import is impaired in cells exposed to poly-GR peptides. Importantly, this effect was not dependent on the presence of SGs, as we did not detect SGs under our assay conditions. Interestingly, we observed striking differences between poly-GR and poly-PR, as poly-PR only marginally interfered with import of the TDP-43 reporter, likely because it is sequestered more strongly than poly-GR by other cellular factors. This finding is in contrast with a previous finding suggesting a general block of NCT by poly-PR due to direct binding of FG-Nups and blocking of the NPC (Shi et al., 2017). Furthermore, our data indicate that poly-GR impairs cNLS-mediated import in general, as also import of TDP-43 lacking the LCD domain or import of MBP-cNLS or a cNLS alone in the context of our hormone-sensitive import reporter was impaired by poly-GR. Diffusion of a reporter protein lacking an NLS across the NPC appeared unaffected or only mildly affected by the presence of poly-GR, suggesting that the import defect is caused predominantly by GR interfering with the functionality of Impα/β and not by affecting TDP-43 directly, blocking the NPC or interfering with our reporter system per se. However, we cannot exclude that the nature of the tag or the large size of our reporter (>100 kDa) promotes the GR-specific import impairment. The latter possibility could explain the discrepancy between our data and that of Vanneste et al. (2019), as larger cargo more strongly depends on active nuclear import (Lyman et al., 2002) and hence might cause a higher sensitivity of our reporter system to treatment with short DPR peptides.

R-Rich DPRs Promote Phase Separation of TDP-43

Enhanced LLPS of RBPs, such as hnRNP-A1, TIA-1, and NPM1, by poly-GR and/or poly-PR has been previously reported (Boeynaems et al., 2017; Lee et al., 2016; Odeh and Shorter, 2020; White et al., 2019), but most of these RBPs have not been linked to C9-ALS/FTD. Our study, along with the work of Cook et al. (2020), reports DPR-induced phase separation of TDP-43, the most prevalent aggregated RBP in C9-ALS/FTD. Here, it is noteworthy that TDP-43, in contrast to other RBPs such as TIA-1, hnRNP-A1, and NPM1, forms irregularly shaped condensates in presence of R-rich DPRs. These condensates do not fuse, nor do they have a round, droplet-like appearance (see also Cook et al., 2020). Instead, TDP-43/GR condensates are amorphous and tend to stick to one another, indicative of a solid-like character. Importantly, we confirmed reduced solubility of endogenous TDP-43 upon addition of poly-GR and poly-PR in intact cells. Altered phase separation behavior of TDP-43 in the presence of poly-GR could contribute to the reduced accessibility of TDP-43 to Impα/β, in addition to the effect of poly-GR on Impα/β, which contributes to impaired Impα/β-dependent TDP-43 import. As reported previously, Impα/β acts as a chaperone, but can also disaggregate, prevent and even revert aberrant phase separation of TDP-43 (Guo et al., 2018). Therefore, the reduced solubility of Impα/β by poly-GR could in turn also negatively affect TDP-43 solubility, thus exacerbating its cytoplasmic mislocalization and related toxicity. This hypothesis is consistent with the recently reported colocalization of TDP-43 with poly-GR in C9-ALS patients or mice (Chew et al., 2019; Cook et al., 2020; Saberi et al., 2018). However, it should be noted that the correlation of DPR inclusions in general with either neurodegeneration or TDP-43 pathology is still controversial and requires further investigation (Mackenzie et al., 2013, 2015; Mann et al., 2013; Saberi et al., 2018; Sakae et al., 2018; Schludi et al., 2015).

Increased Concentration of Importins Can Shield R-Rich DPRs from Pathological Interactions

Interestingly, we found that the outcome of the DPR-importin interaction strongly depends on the molecular ratio of DPRs and importins. Although GR_{25} and PR_{25} peptides in molar excess

over importins result in precipitation and condensation of several importins, sufficiently high concentrations of importins can shield GR_{25} and PR_{25} from engaging in pathological interactions with TDP-43 or with RNA. These findings are in line with previous work demonstrating that importins can suppress phase transitions of aggregation-prone RBPs (Guo et al., 2018; Hofweber et al., 2018; Niaki et al., 2020; Qamar et al., 2018; Yoshizawa et al., 2018) and RNA-mediated aggregation of highly basic ribosomal proteins and histones (Jäkel et al., 2002). Our data now indicate that this chaperoning function extends toward R-rich DPRs, at least *in vitro*, raising the possibility that importins are broadly protective against pathological protein aggregation, particularly in C9-ALS/FTD.

As R-rich DPRs were reported to engage in pathological interactions with various macromolecules and cellular structures (e.g., mitochondria, heterochromatin, ribosomal proteins, and microtubules) (Choi et al., 2019; Fumagalli et al., 2019; Hartmann et al., 2018; Moens et al., 2019; Zhang et al., 2019b), it can be speculated that importins may have the capacity to buffer and suppress, at least to some extent, the pleiotropic poly-GR/PR interactions and hence counteract various pathological effects attributed to R-rich DPRs. Importantly, importins can exert this chaperoning function toward R-rich DPRs not only *in vitro* using recombinant factors, but also prevent GR-induced precipitation of endogenous TDP-43 from the cytosol under physiological cellular conditions. Whether importins can have similar protective effect in C9-patient-derived neurons will need to be investigated.

On the basis of our findings, two possible, non-mutually exclusive scenarios exist in C9orf72-linked ALS/FTD. On one hand, R-rich DPRs could sequester importins and hence result in cellular toxicity. On the other hand, reduced levels or reduced availability of import receptors could potentiate toxicity of R-rich DPRs. Notably, expression of an Impα isoform, CAS and RanBP17 were found to be reduced in C9-ALS/FTD or aging fibroblasts and aged-preserved induced neurons (Mertens et al., 2015; Nishimura et al., 2010; Pujol et al., 2002). Whether expression levels of other NTRs are also changed in the aging or diseased brain, for example in specific brain regions or vulnerable cell types, has not yet been directly addressed. Reduced importin levels during physiological aging could have direct implications for neurodegeneration in C9-ALS/FTD. Reduced importin levels could shift the DPR-importin ratio in a way that reduces the availability of import receptors, thereby promoting insolubility of certain RBPs and abrogating the chaperoning of R-rich DPRs and RBPs alike by import receptors. This effect, in turn, is expected to cause defective nuclear import of certain RBPs, RBP aggregation, and pathological interactions with other cellular structures (Boeynaems et al., 2016b, 2017; Choi et al., 2019; Fumagalli et al., 2019; Hartmann et al., 2018; Jovičić et al., 2015; Kim and Taylor, 2017; Lin et al., 2016; Moens et al., 2019; Shi et al., 2017; White et al., 2019; Yin et al., 2017; Zhang et al., 2016), contributing to neuronal dysfunction and neurodegeneration.

Importantly, however, our findings could have therapeutic implications, as they suggest that increasing the concentrations of import receptors or enhancing their performance toward aggregation-prone target molecules, might be a promising therapeutic approach in the treatment of C9-ALS/FTD (Guo et al., 2019).

STAR★METHODS

Detailed methods are provided in the online version of this paper and include the following:

- KEY RESOURCES TABLE
- RESOURCE AVAILABILITY
  - Lead Contact
  - Materials Availability
  - Data and Code Availability
- EXPERIMENTAL MODEL AND SUBJECT DETAILS
- METHOD DETAILS
  - Transfection and viral transductions
  - Peptides
  - DNA constructs
  - Preparation of total RNA
  - Preparation of HeLa cytosol
  - Recombinant protein expression and purification
  - GST and GST-DPRs
  - (His_6)-TNPO1 and His_6-TNPO3
  - His_6-GFP-TNPO1
  - GST-Tev-TNPO1
  - His_6-S-Impβ and His_6-GFP-Impβ
  - His_6-Impα1 and His_6-Impα3
  - CRM1
  - TDP-43-Tev-MBP-His_6
  - MBP- Tev-TDP-43-GFP-Tev-His_6
  - His_6-Tev
  - Biotin-DPR Pulldowns
  - Fluorescence Polarization Measurements
  - SAXS
  - *In vitro* phase separation assays
  - Sedimentation assay
  - Visualization of condensates by microscopy
  - Analysis of oligomer formation by SDD-AGE
  - Turbidity assay
  - Solubility assay of endogenous TDP-43 by RIPA extraction
  - Immunocytochemistry
  - Nuclear transport assay (Hormone-induced import assay)
- MICROSCOPY
  - Laser scanning confocal microscopy
  - Spinning disc confocal live cell microscopy
  - Fluorescence Recovery after Photobleaching (FRAP)
- QUANTIFICATION AND STATISTICAL ANALYSIS
  - Microscopy
  - FRAP analysis of cytoplasmic GCR_2-GFP_2 dynamics
  - Densitometry measurements (Sypro-Ruby, western blot)

SUPPLEMENTAL INFORMATION

Supplemental Information can be found online at https://doi.org/10.1016/j.celrep.2020.108538.

ACKNOWLEDGMENTS

We thank Erin Sternburg and Lara Gruijs da Silva for critical comments on the manuscript and helpful discussions and Annika Niedner-Boblenz, Claudia Abou-Ajram, Lara Gruijs da Silva, and Moritz Völker-Albert for technical assistance with cell culture, cloning, and protein purifications. We thank Ralph Kehlenbach, Arie Geerlof, Marc Ruepp, Dirk Görlich, Dierk Niessing, Angus Lamond, Axel Imhoff, Moritz Völker-Albert, and Michael Kiebler for the generous gift of reagents. We thank Peter Becker and the BioMedical Center Core Facilities Bioimaging and Bioinformatics for support. We acknowledge Michael Kiebler for access to spinning disc confocal microscope (DFG, INST 86/1581-1 FUGG) and the ZMF for access to their facilities. This work was supported by the Fritz Thyssen Foundation (Az. 10.19.1.001MN, to D.D.), Deutsche Forschungsgemeinschaft (DFG; German Research Foundation) within Emmy Noether grants DO 1804/1-1 and DO 1804/1-2 (to D.D.), the Munich Cluster for Systems Neurology (EXC2145 SyNergy – ID 390857198 to D.D. and D.E.), the Junior Researcher Fund of Ludwig-Maximilians-Universität München (to D.D.), the NOMIS Foundation (to D.E.), the Austrian Science Foundation (P28854, I3792, DK-MCD W1226 to T.M.), the Austrian Research Promotion Agency (FFG: 864690, 870454 to T.M.), the Integrative Metabolism Research Center Graz, the Austrian infrastructure program 2016/2017 (to T.M.), the Styrian government (Zukunftsfonds, to T.M.), and BioTechMed/Graz (flagship project, to T.M.). C.M.F. was supported by NIH grants T32GM008275 and F31NS111870. J.S. was supported by NIH grant R21NS090205, the G. Harold and Leila Y. Mathers Charitable Foundation, Target ALS, ALSA, and the Packard Center for ALS Research. M.P. was supported by the Swiss National Science Foundation, Target ALS, ALSA, and the Association for Frontotemporal Degeneration (AFTD). S.U. was trained within the framework of the PhD program Metabolic and Cardiovascular Disease (DK-MCD) and M.H. in the Graduate School of Systemic Neurosciences Munich. H.M.O. was supported by an AstraZeneca postdoctoral fellowship.

AUTHOR CONTRIBUTIONS

Conceptualization, S.H. and D.D.; Methodology, S.H., F.S., S.U., C.M.F., H.M.O., M.C., B.B., M.H.-P., M.H., T.M., J.S., D.E., and D.D.; Investigation, S.H., F.S., S.U., B.B., H.M.O., C.M.F., M.C., M.H., and M.H.-P.; Resources, T.M., J.S., D.E., M.P., and D.D.; Writing – Original Draft, S.H. and D.D.; Writing – Review & Editing, D.D., S.H., D.E., M.H.-P., H.M.O., C.M.F., J.S., B.B., and T.M.; Visualization, S.H., S.U., H.M.O.; B.B., T.M., J.S., and D.D.; Supervision, D.D.; Project Administration, D.D.; Funding Acquisition, D.D.

DECLARATION OF INTERESTS

J.S. is a consultant for Dewpoint Therapeutics.

Received: August 10, 2020
Revised: November 6, 2020
Accepted: November 25, 2020
Published: December 22, 2020

REFERENCES

Ash, P.E., Bieniek, K.F., Gendron, T.F., Caulfield, T., Lin, W.L., Dejesus-Hernandez, M., van Blitterswijk, M.M., Jansen-West, K., Paul, J.W., 3rd, Rademakers, R., et al. (2013). Unconventional translation of C9ORF72 GGGGCC expansion generates insoluble polypeptides specific to c9FTD/ALS. Neuron *77*, 639–646.

Askjaer, P., Bachi, A., Wilm, M., Bischoff, F.R., Weeks, D.L., Ogniewski, V., Ohno, M., Niehrs, C., Kjems, J., Mattaj, I.W., and Fornerod, M. (1999). RanGTP-regulated interactions of CRM1 with nucleoporins and a shuttling DEAD-box helicase. Mol. Cell. Biol. *19*, 6276–6285.

Balendra, R., and Isaacs, A.M. (2018). C9orf72-mediated ALS and FTD: multiple pathways to disease. Nat. Rev. Neurol. *14*, 544–558.

Boeynaems, S., Bogaert, E., Michiels, E., Gijselinck, I., Sieben, A., Jovičić, A., De Baets, G., Scheveneels, W., Steyaert, J., Cuijt, I., et al. (2016a). Drosophila screen connects nuclear transport genes to DPR pathology in c9ALS/FTD. Sci. Rep. *6*, 20877.

Boeynaems, S., Bogaert, E., Van Damme, P., and Van Den Bosch, L. (2016b). Inside out: the role of nucleocytoplasmic transport in ALS and FTLD. Acta Neuropathol. *132*, 159–173.

Boeynaems, S., Bogaert, E., Kovacs, D., Konijnenberg, A., Timmerman, E., Volkov, A., Guharoy, M., De Decker, M., Jaspers, T., Ryan, V.H., et al. (2017). Phase separation of C9orf72 dipeptide repeats perturbs stress granule dynamics. Mol. Cell *65*, 1044–1055.e5.

Boeynaems, S., Holehouse, A.S., Weinhardt, V., Kovacs, D., Van Lindt, J., Larabell, C., Van Den Bosch, L., Das, R., Tompa, P.S., Pappu, R.V., and Gitler, A.D. (2019). Spontaneous driving forces give rise to protein-RNA condensates with coexisting phases and complex material properties. Proc. Natl. Acad. Sci. U S A *116*, 7889–7898.

Bourgeois, B., Hutten, S., Gottschalk, B., Hofweber, M., Richter, G., Sternat, J., Abou-Ajram, C., Göbl, C., Leitinger, G., Graier, W.F., et al. (2020). Nonclassical nuclear localization signals mediate nuclear import of CIRBP. Proc. Natl. Acad. Sci. U S A *117*, 8503–8514.

Cansizoglu, A.E., Lee, B.J., Zhang, Z.C., Fontoura, B.M., and Chook, Y.M. (2007). Structure-based design of a pathway-specific nuclear import inhibitor. Nat. Struct. Mol. Biol. *14*, 452–454.

Chew, J., Cook, C., Gendron, T.F., Jansen-West, K., Del Rosso, G., Daughrity, L.M., Castanedes-Casey, M., Kurti, A., Stankowski, J.N., Disney, M.D., et al. (2019). Aberrant deposition of stress granule-resident proteins linked to C9orf72-associated TDP-43 proteinopathy. Mol. Neurodegener. *14*, 9.

Chi, N.C., Adam, E.J., and Adam, S.A. (1997). Different binding domains for Ran-GTP and Ran-GDP/RanBP1 on nuclear import factor p97. J. Biol. Chem. *272*, 6818–6822.

Choi, S.Y., Lopez-Gonzalez, R., Krishnan, G., Phillips, H.L., Li, A.N., Seeley, W.W., Yao, W.D., Almeida, S., and Gao, F.B. (2019). C9ORF72-ALS/FTD-associated poly(GR) binds Atp5a1 and compromises mitochondrial function in vivo. Nat. Neurosci. *22*, 851–862.

Chook, Y.M., and Blobel, G. (1999). Structure of the nuclear transport complex karyopherin-beta2-Ran x GppNHp. Nature *399*, 230–237.

Christie, M., Chang, C.W., Róna, G., Smith, K.M., Stewart, A.G., Takeda, A.A., Fontes, M.R., Stewart, M., Vértessy, B.G., Forwood, J.K., and Kobe, B. (2016). Structural biology and regulation of protein import into the nucleus. J. Mol. Biol. *428* (*10 Pt A*), 2060–2090.

Cook, C.N., Wu, Y., Odeh, H.M., Gendron, T.F., Jansen-West, K., Del Rosso, G., Yue, M., Jiang, P., Gomes, E., Tong, J., et al. (2020). *C9orf72* poly(GR) aggregation induces TDP-43 proteinopathy. Sci. Transl. Med. *12*, eabb3774.

DeJesus-Hernandez, M., Mackenzie, I.R., Boeve, B.F., Boxer, A.L., Baker, M., Rutherford, N.J., Nicholson, A.M., Finch, N.A., Flynn, H., Adamson, J., et al. (2011). Expanded GGGGCC hexanucleotide repeat in noncoding region of C9ORF72 causes chromosome 9p-linked FTD and ALS. Neuron *72*, 245–256.

Dormann, D., and Haass, C. (2011). TDP-43 and FUS: a nuclear affair. Trends Neurosci. *34*, 339–348.

Dormann, D., Rodde, R., Edbauer, D., Bentmann, E., Fischer, I., Hruscha, A., Than, M.E., Mackenzie, I.R., Capell, A., Schmid, B., et al. (2010). ALS-associated fused in sarcoma (FUS) mutations disrupt Transportin-mediated nuclear import. EMBO J. *29*, 2841–2857.

Ederle, H., Funk, C., Abou-Ajram, C., Hutten, S., Funk, E.B.E., Kehlenbach, R.H., Bailer, S.M., and Dormann, D. (2018). Nuclear egress of TDP-43 and FUS occurs independently of Exportin-1/CRM1. Sci Rep *8*, 7084.

Freibaum, B.D., Lu, Y., Lopez-Gonzalez, R., Kim, N.C., Almeida, S., Lee, K.H., Badders, N., Valentine, M., Miller, B.L., Wong, P.C., et al. (2015). GGGGCC repeat expansion in C9orf72 compromises nucleocytoplasmic transport. Nature *525*, 129–133.

French, R.L., Grese, Z.R., Aligireddy, H., Dhavale, D.D., Reeb, A.N., Kedia, N., Kotzbauer, P.T., Bieschke, J., and Ayala, Y.M. (2019). Detection of TAR DNA-binding protein 43 (TDP-43) oligomers as initial intermediate species during aggregate formation. J. Biol. Chem. *294*, 6696–6709.

Frey, S., Rees, R., Schunemann, J., Ng, S.C., Funfgeld, K., Huyton, T., and Gorlich, D. (2018). Surface properties determining passage rates of proteins through nuclear pores. Cell *174*, 202–217.e9.

Frohnert, C., Hutten, S., Wälde, S., Nath, A., and Kehlenbach, R.H. (2014). Importin 7 and Nup358 promote nuclear import of the protein component of human telomerase. PLoS ONE *9*, e88887.

Fumagalli, L., Young, F.L., Boeynaems, S., Decker, M.D., Mehta, A.R., Swijsen, A., Fazal, R., Guo, W., Moisse, M., Beckers, J., et al. (2019). *C9orf72*-derived arginine-containing dipeptide repeats associate with axonal transport machinery and impede microtubule-based motility. bioRxiv. https://doi.org/10.1101/835082.

Gendron, T.F., Bieniek, K.F., Zhang, Y.J., Jansen-West, K., Ash, P.E., Caulfield, T., Daughrity, L., Dunmore, J.H., Castanedes-Casey, M., Chew, J., et al. (2013). Antisense transcripts of the expanded C9ORF72 hexanucleotide repeat form nuclear RNA foci and undergo repeat-associated non-ATG translation in c9FTD/ALS. Acta Neuropathol. *126*, 829–844.

Gittings, L.M., Boeynaems, S., Lightwood, D., Clargo, A., Topia, S., Nakayama, L., Troakes, C., Mann, D.M.A., Gitler, A.D., Lashley, T., and Isaacs, A.M. (2020). Symmetric dimethylation of poly-GR correlates with disease duration in C9orf72 FTLD and ALS and reduces poly-GR phase separation and toxicity. Acta Neuropathol. *139*, 407–410.

Guo, L., Kim, H.J., Wang, H., Monaghan, J., Freyermuth, F., Sung, J.C., O'Donovan, K., Fare, C.M., Diaz, Z., Singh, N., et al. (2018). Nuclear-import receptors reverse aberrant phase transitions of RNA-binding proteins with prion-like domains. Cell *173*, 677–692.e20.

Guo, L., Fare, C.M., and Shorter, J. (2019). Therapeutic dissolution of aberrant phases by nuclear-import receptors. Trends Cell Biol. *29*, 308–322.

Güttler, T., Madl, T., Neumann, P., Deichsel, D., Corsini, L., Monecke, T., Ficner, R., Sattler, M., and Görlich, D. (2010). NES consensus redefined by structures of PKI-type and Rev-type nuclear export signals bound to CRM1. Nat. Struct. Mol. Biol. *17*, 1367–1376.

Halfmann, R., and Lindquist, S. (2008). Screening for amyloid aggregation by semi-denaturing detergent-agarose gel electrophoresis. J. Vis. Exp. (*17*), 838.

Hartmann, H., Hornburg, D., Czuppa, M., Bader, J., Michaelsen, M., Farny, D., Arzberger, T., Mann, M., Meissner, F., and Edbauer, D. (2018). Proteomics and *C9orf72* neuropathology identify ribosomes as poly-GR/PR interactors driving toxicity. Life Sci. Alliance *1*, e201800070.

Hayes, L.R., Duan, L., Bowen, K., Kalab, P., and Rothstein, J.D. (2019). C9orf72 arginine-rich dipeptide repeat proteins disrupt importin β-mediated nuclear import. bioRxiv. https://doi.org/10.1101/787473.

Hayes, L.R., Duan, L., Bowen, K., Kalab, P., and Rothstein, J.D. (2020). *C9orf72* arginine-rich dipeptide repeat proteins disrupt karyopherin-mediated nuclear import. eLife *9*, e51685.

Hofweber, M., Hutten, S., Bourgeois, B., Spreitzer, E., Niedner-Boblenz, A., Schifferer, M., Ruepp, M.D., Simons, M., Niessing, D., Madl, T., et al. (2018). Phase separation of FUS is suppressed by its nuclear import receptor and arginine methylation. Cell *173*, 706–719.e13.

Hutten, S., Flotho, A., Melchior, F., and Kehlenbach, R.H. (2008). The Nup358-RanGAP complex is required for efficient importin alpha/beta-dependent nuclear import. Mol Biol Cell *19*, 2300–2310.

Jäkel, S., Mingot, J.M., Schwarzmaier, P., Hartmann, E., and Görlich, D. (2002). Importins fulfil a dual function as nuclear import receptors and cytoplasmic chaperones for exposed basic domains. EMBO J. *21*, 377–386.

Jovičić, A., Mertens, J., Boeynaems, S., Bogaert, E., Chai, N., Yamada, S.B., Paul, J.W., 3rd, Sun, S., Herdy, J.R., Bieri, G., et al. (2015). Modifiers of C9orf72 dipeptide repeat toxicity connect nucleocytoplasmic transport defects to FTD/ALS. Nat. Neurosci. *18*, 1226–1229.

Khosravi, B., Hartmann, H., May, S., Möhl, C., Ederle, H., Michaelsen, M., Schludi, M.H., Dormann, D., and Edbauer, D. (2017). Cytoplasmic poly-GA aggregates impair nuclear import of TDP-43 in C9orf72 ALS/FTLD. Hum. Mol. Genet. *26*, 790–800.

Kim, H.J., and Taylor, J.P. (2017). Lost in transportation: nucleocytoplasmic transport defects in ALS and other neurodegenerative diseases. Neuron *96*, 285–297.

Kramer, N.J., Haney, M.S., Morgens, D.W., Jovičić, A., Couthouis, J., Li, A., Ousey, J., Ma, R., Bieri, G., Tsui, C.K., et al. (2018). CRISPR-Cas9 screens in human cells and primary neurons identify modifiers of C9ORF72 dipeptide-repeat-protein toxicity. Nat. Genet. *50*, 603–612.

Kwon, I., Xiang, S., Kato, M., Wu, L., Theodoropoulos, P., Wang, T., Kim, J., Yun, J., Xie, Y., and McKnight, S.L. (2014). Poly-dipeptides encoded by the C9orf72 repeats bind nucleoli, impede RNA biogenesis, and kill cells. Science *345*, 1139–1145.

Lafarga, V., Sirozh, O., Díaz-López, I., Hisaoka, M., Zarzuela, E., Boskovic, J., Jovanovic, B., Fernandez-Leiro, R., Muñoz, J., Stoecklin, G., et al. (2019). Generalized displacement of DNA- and RNA-binding factors mediates the toxicity of arginine-rich cell-penetrating peptides. bioRxiv. https://doi.org/10.1101/441808.

Lee, K.H., Zhang, P., Kim, H.J., Mitrea, D.M., Sarkar, M., Freibaum, B.D., Cika, J., Coughlin, M., Messing, J., Molliex, A., et al. (2016). C9orf72 dipeptide repeats impair the assembly, dynamics, and function of membrane-less organelles. Cell *167*, 774–788.e17.

Lin, Y., Protter, D.S., Rosen, M.K., and Parker, R. (2015). Formation and maturation of phase-separated liquid droplets by RNA-binding proteins. Mol. Cell *60*, 208–219.

Lin, Y., Mori, E., Kato, M., Xiang, S., Wu, L., Kwon, I., and McKnight, S.L. (2016). Toxic PR poly-dipeptides encoded by the C9orf72 repeat expansion target LC domain polymers. Cell *167*, 789–802.e12.

Ling, S.C., Polymenidou, M., and Cleveland, D.W. (2013). Converging mechanisms in ALS and FTD: disrupted RNA and protein homeostasis. Neuron *79*, 416–438.

Lott, K., and Cingolani, G. (2011). The importin β binding domain as a master regulator of nucleocytoplasmic transport. Biochim. Biophys. Acta *1813*, 1578–1592.

Love, D.C., Sweitzer, T.D., and Hanover, J.A. (1998). Reconstitution of HIV-1 rev nuclear export: independent requirements for nuclear import and export. Proc. Natl. Acad. Sci. U S A *95*, 10608–10613.

Lyman, S.K., Guan, T., Bednenko, J., Wodrich, H., and Gerace, L. (2002). Influence of cargo size on Ran and energy requirements for nuclear protein import. J. Cell Biol. *159*, 55–67.

Mackenzie, I.R., Arzberger, T., Kremmer, E., Troost, D., Lorenzl, S., Mori, K., Weng, S.M., Haass, C., Kretzschmar, H.A., Edbauer, D., and Neumann, M. (2013). Dipeptide repeat protein pathology in C9ORF72 mutation cases: clinico-pathological correlations. Acta Neuropathol. *126*, 859–879.

Mackenzie, I.R., Frick, P., Grässer, F.A., Gendron, T.F., Petrucelli, L., Cashman, N.R., Edbauer, D., Kremmer, E., Prudlo, J., Troost, D., and Neumann, M. (2015). Quantitative analysis and clinico-pathological correlations of different dipeptide repeat protein pathologies in C9ORF72 mutation carriers. Acta Neuropathol. *130*, 845–861.

Mann, D.M., Rollinson, S., Robinson, A., Bennion Callister, J., Thompson, J.C., Snowden, J.S., Gendron, T., Petrucelli, L., Masuda-Suzukake, M., Hasegawa, M., et al. (2013). Dipeptide repeat proteins are present in the p62 positive inclusions in patients with frontotemporal lobar degeneration and motor neurone disease associated with expansions in C9ORF72. Acta Neuropathol. Commun. *1*, 68.

Mertens, J., Paquola, A.C.M., Ku, M., Hatch, E., Böhnke, L., Ladjevardi, S., McGrath, S., Campbell, B., Lee, H., Herdy, J.R., et al. (2015). Directly reprogrammed human neurons retain aging-associated transcriptomic signatures and reveal age-related nucleocytoplasmic defects. Cell Stem Cell *17*, 705–718.

Milles, S., Huy Bui, K., Koehler, C., Eltsov, M., Beck, M., and Lemke, E.A. (2013). Facilitated aggregation of FG nucleoporins under molecular crowding conditions. EMBO Rep. *14*, 178–183.

Mizielinska, S., Ridler, C.E., Balendra, R., Thoeng, A., Woodling, N.S., Grässer, F.A., Plagnol, V., Lashley, T., Partridge, L., and Isaacs, A.M. (2017).

Bidirectional nucleolar dysfunction in C9orf72 frontotemporal lobar degeneration. Acta Neuropathol. Commun. *5*, 29.

Moens, T.G., Niccoli, T., Wilson, K.M., Atilano, M.L., Birsa, N., Gittings, L.M., Holbling, B.V., Dyson, M.C., Thoeng, A., Neeves, J., et al. (2019). C9orf72 arginine-rich dipeptide proteins interact with ribosomal proteins in vivo to induce a toxic translational arrest that is rescued by eIF1A. Acta Neuropathol. *137*, 487–500.

Moerke, N.J. (2009). Fluorescence polarization (FP) assays for monitoring peptide-protein or nucleic acid-protein binding. Curr. Protoc. Chem. Biol. *1*, 1–15.

Molliex, A., Temirov, J., Lee, J., Coughlin, M., Kanagaraj, A.P., Kim, H.J., Mittag, T., and Taylor, J.P. (2015). Phase separation by low complexity domains promotes stress granule assembly and drives pathological fibrillization. Cell *163*, 123–133.

Mori, K., Weng, S.M., Arzberger, T., May, S., Rentzsch, K., Kremmer, E., Schmid, B., Kretzschmar, H.A., Cruts, M., Van Broeckhoven, C., et al. (2013). The C9orf72 GGGGCC repeat is translated into aggregating dipeptide-repeat proteins in FTLD/ALS. Science *339*, 1335–1338.

Murakami, T., Qamar, S., Lin, J.Q., Schierle, G.S., Rees, E., Miyashita, A., Costa, A.R., Dodd, R.B., Chan, F.T., Michel, C.H., et al. (2015). ALS/FTD mutation-induced phase transition of FUS liquid droplets and reversible hydrogels into irreversible hydrogels impairs RNP granule function. Neuron *88*, 678–690.

Murray, M.E., DeJesus-Hernandez, M., Rutherford, N.J., Baker, M., Duara, R., Graff-Radford, N.R., Wszolek, Z.K., Ferman, T.J., Josephs, K.A., Boylan, K.B., et al. (2011). Clinical and neuropathologic heterogeneity of c9FTD/ALS associated with hexanucleotide repeat expansion in C9ORF72. Acta Neuropathol. *122*, 673–690.

Niaki, A.G., Sarkar, J., Cai, X., Rhine, K., Vidaurre, V., Guy, B., Hurst, M., Lee, J.C., Koh, H.R., Guo, L., et al. (2020). Loss of dynamic RNA interaction and aberrant phase separation induced by two distinct types of ALS/FTD-linked FUS mutations. Mol. Cell *77*, 82–94.e4.

Nishimura, A.L., Zupunski, V., Troakes, C., Kathe, C., Fratta, P., Howell, M., Gallo, J.M., Hortobágyi, T., Shaw, C.E., and Rogelj, B. (2010). Nuclear import impairment causes cytoplasmic trans-activation response DNA-binding protein accumulation and is associated with frontotemporal lobar degeneration. Brain *133*, 1763–1771.

Odeh, H.M., and Shorter, J. (2020). Arginine-rich dipeptide-repeat proteins as phase disruptors in C9-ALS/FTD. Emerg. Top. Life Sci. Published online July 8, 2020. https://doi.org/10.1042/ETLS20190167.

Patel, A., Lee, H.O., Jawerth, L., Maharana, S., Jahnel, M., Hein, M.Y., Stoynov, S., Mahamid, J., Saha, S., Franzmann, T.M., et al. (2015). A liquid-to-solid phase transition of the ALS protein FUS accelerated by disease mutation. Cell *162*, 1066–1077.

Pujol, G., Söderqvist, H., and Radu, A. (2002). Age-associated reduction of nuclear protein import in human fibroblasts. Biochem. Biophys. Res. Commun. *294*, 354–358.

Qamar, S., Wang, G., Randle, S.J., Ruggeri, F.S., Varela, J.A., Lin, J.Q., Phillips, E.C., Miyashita, A., Williams, D., Strohl, F., et al. (2018). FUS phase separation is modulated by a molecular chaperone and methylation of arginine cation-pi interactions. Cell *173*, 720–734.e15.

Renton, A.E., Majounie, E., Waite, A., Simón-Sánchez, J., Rollinson, S., Gibbs, J.R., Schymick, J.C., Laaksovirta, H., van Swieten, J.C., Myllykangas, L., et al.; ITALSGEN Consortium (2011). A hexanucleotide repeat expansion in C9ORF72 is the cause of chromosome 9p21-linked ALS-FTD. Neuron *72*, 257–268.

Roloff, S., Spillner, C., and Kehlenbach, R.H. (2013). Several phenylalanine-glycine motives in the nucleoporin Nup214 are essential for binding of the nuclear export receptor CRM1. J. Biol. Chem. *288*, 3952–3963.

Saberi, S., Stauffer, J.E., Jiang, J., Garcia, S.D., Taylor, A.E., Schulte, D., Ohkubo, T., Schloffman, C.L., Maldonado, M., Baughn, M., et al. (2018). Sense-encoded poly-GR dipeptide repeat proteins correlate to neurodegeneration and uniquely co-localize with TDP-43 in dendrites of repeat-expanded C9orf72 amyotrophic lateral sclerosis. Acta Neuropathol. *135*, 459–474.

Sakae, N., Bieniek, K.F., Zhang, Y.J., Ross, K., Gendron, T.F., Murray, M.E., Rademakers, R., Petrucelli, L., and Dickson, D.W. (2018). Poly-GR dipeptide repeat polymers correlate with neurodegeneration and Clinicopathological subtypes in C9ORF72-related brain disease. Acta Neuropathol. Commun. *6*, 63.

Schludi, M.H., May, S., Grässer, F.A., Rentzsch, K., Kremmer, E., Küpper, C., Klopstock, T., Arzberger, T., and Edbauer, D.German Consortium for Frontotemporal Lobar Degeneration; Bavarian Brain Banking Alliance (2015). Distribution of dipeptide repeat proteins in cellular models and C9orf72 mutation cases suggests link to transcriptional silencing. Acta Neuropathol. *130*, 537–555.

Shi, K.Y., Mori, E., Nizami, Z.F., Lin, Y., Kato, M., Xiang, S., Wu, L.C., Ding, M., Yu, Y., Gall, J.G., and McKnight, S.L. (2017). Toxic PR_n poly-dipeptides encoded by the *C9orf72* repeat expansion block nuclear import and export. Proc. Natl. Acad. Sci. U S A *114*, E1111–E1117.

Simón-Sánchez, J., Dopper, E.G., Cohn-Hokke, P.E., Hukema, R.K., Nicolaou, N., Seelaar, H., de Graaf, J.R., de Koning, I., van Schoor, N.M., Deeg, D.J., et al. (2012). The clinical and pathological phenotype of C9ORF72 hexanucleotide repeat expansions. Brain *135*, 723–735.

Solomon, D.A., Stepto, A., Au, W.H., Adachi, Y., Diaper, D.C., Hall, R., Rekhi, A., Boudi, A., Tziortzouda, P., Lee, Y.B., et al. (2018). A feedback loop between dipeptide-repeat protein, TDP-43 and karyopherin-α mediates C9orf72-related neurodegeneration. Brain *141*, 2908–2924.

Stewart, H., Rutherford, N.J., Briemberg, H., Krieger, C., Cashman, N., Fabros, M., Baker, M., Fok, A., DeJesus-Hernandez, M., Eisen, A., et al. (2012). Clinical and pathological features of amyotrophic lateral sclerosis caused by mutation in the C9ORF72 gene on chromosome 9p. Acta Neuropathol. *123*, 409–417.

Suárez-Calvet, M., Neumann, M., Arzberger, T., Abou-Ajram, C., Funk, E., Hartmann, H., Edbauer, D., Kremmer, E., Göbl, C., Resch, M., et al. (2016). Monomethylated and unmethylated FUS exhibit increased binding to Transportin and distinguish FTLD-FUS from ALS-FUS. Acta Neuropathol. *131*, 587–604.

Swinnen, B., Robberecht, W., and Van Den Bosch, L. (2019). RNA toxicity in non-coding repeat expansion disorders. EMBO J. *39*, e101112.

Tao, Z., Wang, H., Xia, Q., Li, K., Li, K., Jiang, X., Xu, G., Wang, G., and Ying, Z. (2015). Nucleolar stress and impaired stress granule formation contribute to C9orf72 RAN translation-induced cytotoxicity. Hum. Mol. Genet. *24*, 2426–2441.

Taylor, J.P., Brown, R.H., Jr., and Cleveland, D.W. (2016). Decoding ALS: from genes to mechanism. Nature *539*, 197–206.

Vanneste, J., Vercruysse, T., Boeynaems, S., Sicart, A., Van Damme, P., Daelemans, D., and Van Den Bosch, L. (2019). C9orf72-generated poly-GR and poly-PR do not directly interfere with nucleocytoplasmic transport. Sci. Rep. *9*, 15728.

Wang, A., Conicella, A.E., Schmidt, H.B., Martin, E.W., Rhoads, S.N., Reeb, A.N., Nourse, A., Ramirez Montero, D., Ryan, V.H., Rohatgi, R., et al. (2018). A single N-terminal phosphomimic disrupts TDP-43 polymerization, phase separation, and RNA splicing. EMBO J. *37*, e97452.

Webster, C.P., Smith, E.F., Grierson, A.J., and De Vos, K.J. (2018). C9orf72 plays a central role in Rab GTPase-dependent regulation of autophagy. Small GTPases *9*, 399–408.

Weis, K., Mattaj, I.W., and Lamond, A.I. (1995). Identification of hSRP1 alpha as a functional receptor for nuclear localization sequences. Science *268*, 1049–1053.

Wen, X., Tan, W., Westergard, T., Krishnamurthy, K., Markandaiah, S.S., Shi, Y., Lin, S., Shneider, N.A., Monaghan, J., Pandey, U.B., et al. (2014). Antisense proline-arginine RAN dipeptides linked to C9ORF72-ALS/FTD form toxic nuclear aggregates that initiate in vitro and in vivo neuronal death. Neuron *84*, 1213–1225.

White, M.R., Mitrea, D.M., Zhang, P., Stanley, C.B., Cassidy, D.E., Nourse, A., Phillips, A.H., Tolbert, M., Taylor, J.P., and Kriwacki, R.W. (2019). C9orf72 poly(PR) dipeptide repeats disturb biomolecular phase separation and disrupt nucleolar function. Mol. Cell *74*, 713–728.e6.

Winton, M.J., Igaz, L.M., Wong, M.M., Kwong, L.K., Trojanowski, J.Q., and Lee, V.M. (2008). Disturbance of nuclear and cytoplasmic TAR DNA-binding protein (TDP-43) induces disease-like redistribution, sequestration, and aggregate formation. J. Biol. Chem. *283*, 13302–13309.

Yin, S., Lopez-Gonzalez, R., Kunz, R.C., Gangopadhyay, J., Borufka, C., Gygi, S.P., Gao, F.B., and Reed, R. (2017). Evidence that C9ORF72 dipeptide repeat proteins associate with U2 snRNP to cause mis-splicing in ALS/FTD patients. Cell Rep. *19*, 2244–2256.

Yoshizawa, T., Ali, R., Jiou, J., Fung, H.Y.J., Burke, K.A., Kim, S.J., Lin, Y., Peeples, W.B., Saltzberg, D., Soniat, M., et al. (2018). Nuclear import receptor inhibits phase separation of FUS through binding to multiple sites. Cell *173*, 693–705.e22.

Zhang, K., Donnelly, C.J., Haeusler, A.R., Grima, J.C., Machamer, J.B., Steinwald, P., Daley, E.L., Miller, S.J., Cunningham, K.M., Vidensky, S., et al. (2015). The C9orf72 repeat expansion disrupts nucleocytoplasmic transport. Nature *525*, 56–61.

Zhang, K., Grima, J.C., Rothstein, J.D., and Lloyd, T.E. (2016). Nucleocytoplasmic transport in C9orf72-mediated ALS/FTD. Nucleus *7*, 132–137.

Zhang, K., Daigle, J.G., Cunningham, K.M., Coyne, A.N., Ruan, K., Grima, J.C., Bowen, K.E., Wadhwa, H., Yang, P., Rigo, F., et al. (2018a). Stress granule assembly disrupts nucleocytoplasmic transport. Cell *173*, 958–971.e17.

Zhang, Y.J., Gendron, T.F., Ebbert, M.T.W., O'Raw, A.D., Yue, M., Jansen-West, K., Zhang, X., Prudencio, M., Chew, J., Cook, C.N., et al. (2018b). Poly(GR) impairs protein translation and stress granule dynamics in C9orf72-associated frontotemporal dementia and amyotrophic lateral sclerosis. Nat. Med. *24*, 1136–1142.

Zhang, P., Fan, B., Yang, P., Temirov, J., Messing, J., Kim, H.J., and Taylor, J.P. (2019a). Chronic optogenetic induction of stress granules is cytotoxic and reveals the evolution of ALS-FTD pathology. eLife *8*, e39578.

Zhang, Y.J., Guo, L., Gonzales, P.K., Gendron, T.F., Wu, Y., Jansen-West, K., O'Raw, A.D., Pickles, S.R., Prudencio, M., Carlomagno, Y., et al. (2019b). Heterochromatin anomalies and double-stranded RNA accumulation underlie *C9orf72* poly(PR) toxicity. Science *363*, eaav2606.

STAR★METHODS

KEY RESOURCES TABLE

REAGENT or RESOURCE	SOURCE	IDENTIFIER
Antibodies		
Rabbit anti Importin β	(Frohnert et al., 2014), gift from Ralph Kehlenbach, University of Goettingen	N/A
Mouse anti TNPO1 clone D45	Sigma	Cat# T0825, RRID:AB_262123
Goat anti CRM1	(Roloff et al., 2013), gift from Ralph Kehlenbach, University of Goettingen	N/A
Rabbit anti TDP-43	Proteintech	Cat# 10782-2-AP RRID:AB_615042
Mouse anti TDP-43	Proteintech	Cat# 60019-2-Ig RRID:AB_2200520
Goat anti TIA-1	Santa Cruz	Cat# sc-48371 RRID:AB_628358
Rabbit anti GST	Proteintech	Cat# 10000-0-AP RRID:AB_1104231
Mouse anti His_6	Abcam	Cat# ab18184 RRID:AB_444306
Alexa 647 Donkey anti-goat	Thermo	Cat# A-21447 RRID:AB_141844
IRDye® 680RD Donkey anti-Mouse IgG	LI-COR	Cat# P/N 926-68072 RRID:AB_10953628
IRDye® 800RD Donkey anti-Rabbit IgG	LI-COR	Cat# P/N: 926-32213 RRID:AB_62184
Chemicals, Peptides, and Recombinant Proteins		
GST-GR_{25}	This paper	N/A
TMR-GR_{10}	Pepscan	N/A
TMR-GR_{25}	Genscript; Pepscan	N/A
TMR-PR_{25}	Genscript; Pepscan	N/A
TMR-GP_{25}	Pepscan	N/A
FITC-GR_{25}	PSL	N/A
FITC-PR_{25}	PSL	N/A
Biotin-GR_{25}	PSL	N/A
Biotin-PR_{25}	PSL	N/A
Biotin-GP_{25}	PSL	N/A
GR_{20}-FLAG	DGpeptides	N/A
His_6-*Tev*-TNPO1	(Suárez-Calvet et al., 2016)	N/A
GST-*Tev*-TNPO1	(Lee et al., 2016)	N/A
His_6-S-Impβ	(Chi et al., 1997)	N/A
His_6-Impα1	(Weis et al., 1995), gift from Angus Lamond, University of Dundee	N/A
His_6-Impα3	This paper	N/A
His_6-TNPO3	(Bourgeois et al., 2020)	N/A
His_6-TEV	(Hofweber et al., 2018)	N/A
CRM1	(Askjaer et al., 1999; Güttler et al., 2010)	N/A
TDP-43-*Tev*-MBP-His_6	(Wang et al., 2018)	N/A

(*Continued on next page*)

Continued

REAGENT or RESOURCE	SOURCE	IDENTIFIER
MBP-*Tev*-TDP-43-linker-EGFP-*Tev*-His_6	This paper	N/A
His_6-EGFP-TNPO1	This paper	N/A
His_6-EGFP-Impβ	This paper	N/A
Importin 5	(Jäkel et al., 2002), gift from D. Görlich, MPI for Biophysical Chemistry Goettingen	N/A
Importin 7	(Jäkel et al., 2002), gift from D. Görlich, MPI for Biophysical Chemistry Goettingen	N/A
Importin 9	(Jäkel et al., 2002), gift from D. Görlich, MPI for Biophysical Chemistry Goettingen	N/A
DMEM, high glucose, GutaMAX supplement (HeLa wt)	Thermo	Cat# 61965059
DMEM high glucose (HeLa S3)	Sigma	Cat# D6429
Fluorobrite	Thermo	Cat# A1896701
Opti-Mem	Thermo	Cat# 11058-021
Fetal Bovine Serum, qualified, Brazil	Thermo	Cat# 10270106
Fetal Bovine Serum, dialyzed, US origin	Thermo	Cat# 26400044
Albumin from chicken egg white	Sigma	Cat# A5503
Gentamicin (10 mg/mL)	Thermo	Cat# 15710049
Lipofectamine 2000	Thermo	Cat# 11668019
Aprotinin	Roth	Cat# A162
Leupeptin hemisulfate	Roth	Cat# CN33
Pepstatin A	Roth	Cat# 2936
PMSF	Sigma	Cat# 78830
Protease-Inhibitor Cocktail, EDTA-free	Sigma	Cat# S8830-20Tab
Benzonase	Sigma	Cat# E1014
ProLong Diamond Antifade Mountant	Thermo	Cat# P36965
DAPI	Sigma	Cat# D9542
Dexamethasone	Sigma	Cat# D4902
Tri Reagent	Sigma	Cat# T9424
Sypro-Ruby Protein Gel Stain	Sigma	Cat# S4942
Bacterial and Virus Strains		
BL21-DE3	Gift from D. Niessing, University of Ulm	N/A
BL21_DE3 Rosetta	Gift from D. Niessing, University of Ulm	N/A
BL21-DE3 Rosetta2	Gift from D. Niessing, University of Ulm	N/A
BL21-DE3 Rosetta-LysS	Gift from D. Niessing, University of Ulm	N/A
BL21-CodonPlus(DE3)-RIL	Agilent	Cat# 230245
Stbl2	Gift from M. Kiebler, LMU Munich	N/A
Experimental Models: Cell Lines		
HeLa WT	Gift from Marc-David Ruepp, King's College London	N/A
HeLa S3	Gift of A. Imhoff, LMU Munich	N/A
Recombinant DNA		
pGex3X-GR_{25}	This paper	N/A
petM11-His_6-*Tev*-TNPO1	(Suárez-Calvet et al., 2016)	N/A
pET30a-His-S-Impβ	(Chi et al., 1997), gift from Ralph Kehlenbach; University of Goettingen	N/A
pRSETb-His-Impα3	This paper	N/A
pETM11-$His_{6\text{-}ZZ}$TNPO3	(Bourgeois et al., 2020)	N/A

(*Continued on next page*)

Continued

REAGENT or RESOURCE	SOURCE	IDENTIFIER
His_6-TEV in a pET-24d(+) vector	Gift from A. Geerlof, Helmholtz Center Munich	N/A
His_{10}-zz-*Tev*-CRM1 in pQE70	Askjaer et al., 1999 Güttler et al., 2010	N/A
pJ4M TDP-43-Tev-MBP-His_6	Wang et al., 2018	Addgene #104480
pMal -*Tev*-TDP-43-linker-EGFP-*Tev*-His_6	This paper	N/A
pET28a-His_6-EGFP-TNPO1	This paper	N/A
pET28a-His_6-EGFP-Impβ	This paper	N/A
GCR_2-$EGFP_2$-stop-M9	(Bourgeois et al., 2020), gift from R. Kehlenbach, University of Goettingen	N/A
GCR_2-$EGFP_2$-$cNLS_{SV40}$	(Hutten et al., 2008)	N/A
GCR_2-$EGFP_2$-MBP-$cNLS_{SV40}$	This paper	N/A
GCR_2-$EGFP_2$-TDP-43	(Ederle et al., 2018)	N/A
GCR_2-$EGFP_2$-TDP-43 aa1-260 (ΔLCD)	This paper	N/A
Software and Algorithms		
ImageJ	NIH	https://imagej.nih.gov/ij/download.html RRID:SCR_00307
Image Studio Lite	Li-COR	https://www.licor.com/bio/image-studio-lite/download RRID:SCR_013715
Image Lab version 5.2.1	Bio-Rad Laboratories	https://www.bio-rad.com/en-de/product/image-lab-software?ID=KRE6P5E8Z RRID:SCR_014210
Zen2 blue edition (lite)	Zeiss	http://www.zeiss.de/mikroskopie/downloads.html?vaURL=www.zeiss.de/mikroskopie/downloads/zen.html RRID:SCR_013672
LAS X	Leica	https://www.leica-microsystems.com/products/microscope-software/software-for-life-science-research/las-x-powerful-and-flexible/ RRID:SCR_013673
GraphPad Prism8	GraphPad Software, Ink	RRID:SCR_002798
SAXS analysis package, version 3.0	Anton Paar	https://www.anton-paar.com/de-de/produkte/gruppe/saxs/
GIFT	PCG-Software	N/A
CLARIOstar - Data Analysis (MARS)	BMG Labtech	N/A
Others		
4-well ibidi μ -slide	Ibidi	Cat# 80426
8-well ibidi μ -slide	Ibidi	Cat# 80826
HisTrap FF 1ml	GE Healthcare	Cat# 17-5319-01
GSTrap FF 1ml	GE Healthcare	Cat# 17-5310-01
Glutathione Sepharose FF	GE Healthcare	Cat# 17-5132-01
Ni-NTA agarose	QIAGEN	Cat# 30230
Amylose resin	NEB	Cat# E8021S
Streptavidin Sepharose HP	GE Healthcare	Cat# GE17-5113-01
Hiload 16/600 Superdex 200 pg	GE Healthcare	Cat# GE28-9893-35
HiTrap Q FF column	GE Healthcare	Cat# GE17-5156-01
384well plates	Thermo	Cat# 781906

RESOURCE AVAILABILITY

Lead Contact

Further information and requests for reagents may be directed to and will be fulfilled by the Lead Contact, Dorothee Dormann (dorothee.dormann@med.uni-muenchen.de).

Materials Availability

All unique/stable reagents generated in this study are available from the Lead Contact with a completed Materials Transfer Agreement.

Data and Code Availability

This study did not generate any unique datasets or code.

EXPERIMENTAL MODEL AND SUBJECT DETAILS

HeLa cells were grown in DMEM high glucose GlutaMAX (Invitrogen) supplemented with 10% dialyzed FBS, or 10% standard FBS and 10 μg/ml gentamicin, respectively. HeLa S3 were grown in suspension using DMEM high glucose (Sigma) with 10% standard FBS in spinner flasks. All cells were maintained in a humidified incubator at 37°C with 5% CO2.

To induce stress granule formation by proteasome inhibition, HeLa cells were incubated for 2 h in the presence of 10 μM MG132. TMR-labeled DPRs were directly added once into the cell medium lacking FBS at a final concentration of 10 μM and analyzed after 2 h.

METHOD DETAILS

Transfection and viral transductions

Transient transfections of HeLa cells were performed using Lipofectamine 2000 (Thermo) in the absence of gentamycin. To reduce cellular stress elicited by the transfection reagent, medium was changed after 4-6 h.

For immunostaining, HeLa cells were fixed ~20 h after transfection.

Peptides

Chemically synthesized peptides were obtained as lyophilized powder, dissolved either in milli-Q water (for biotin- and TMR-labeled peptides), 1x PBS (for FLAG-tagged peptides), or in 50 mM Tris (pH 7.5), 200 mM NaCl, 2 mM TCEP, 1 mM $MgCl_2$, 5% glycerol (for FITC-labeled peptides).

DNA constructs

Expression constructs for GST- GR_{25}, was generated by Genscript as codon optimized sequences cloned into EcoRI and SalI sites of a pGex3X-backbone.

For amplification of GST-GR_{25}, a recombinase deficient bacterial strain (Stbl2) was used.

To generate the expression construct His_6-GFP-TNPO1 and -Impβ, the coding sequences of GFP, TNPO1 and Impβ were PCR amplified and cloned into a pET28a-backbone using NheI/BamHI, ApaI/BamHI and BamHI/NotI sites, respectively.

For generation of the expression construct coding for His_6-Impα3, rat Impα3 (98.9% identical to human Impα3) was PCR-amplified from rat cDNA and cloned into XhoI/BamHI sites of pRSETb-backbone.

To generate a construct coding for MBP-*Tev*-TDP-43-GFP-*Tev*-His_6, the GFP-*Tev*-His_6 cassette was transferred from MBP-FUS-GFP-His_6 (Hofweber et al., 2018) via BamHI/HindIII into a pMal-C2 backbone containing a Tev-cleavage site downstream of the MBP. Subsequently, the coding sequence of TDP-43 was inserted into the BamHI site. Note that we included a low-complexity linker between TDP-43 and GFP to reduce disturbance of the TDP-43 C terminus by the GFP-fusion. To generate GCR_2-GFP_2-TDP-43 lacking the LCD domain (GCR_2-GFP_2-TDP-43 aa1-260) and GCR_2-GFP_2-MBP-cNLS, the respective coding sequences were PCR amplified and inserted using EcoRV and BamHI.

Preparation of total RNA

Total RNA was purified from HeLa cells using Tri-Reagent (Sigma) and stored in RNase-free milli-Q water at −80°C.

Preparation of HeLa cytosol

HeLa cytosol was either prepared form adherent HeLa cells or HeLa S3 cells grown in suspension. Adhaerent HeLa cells (~0.5-1x10^8 cells) were harvested by trypsinization and washed in transport buffer (TPB; 20 mM HEPES pH 7.3-7.4, 110 mM KAc, 2 mM $Mg(Ac)_2$, 1 mM EGTA supplemented with protease inhibitors and 2mM DTT). Cells were resuspended in equal volume of TPB and the plasma membrane selectively was permeabilized using digitonin. Successful permeabilization was controlled by trypan blue staining. Nuclei were separated from cytosol by centrifugation at 300 g for 5 min at 4°C, and the obtained cytosol subsequently cleared at 21,000 g for

10 min at 4°C. For cytosol derived from HeLa cells grown in suspension, the cells were grown to mid-log phase and collected by centrifugation. After several washes in PBS and once in TPB, celles were resuspended in 1 volume of lysis buffer (5 mM HEPES-KOH pH 7.3, 10 mM K-acetate, 2 mM Mg-acetate supplemented with 1 mM PMSF, 2 mM DTT and 1 μg/ml each of aprotinin, pepstatin and leupeptin. Cells were allowed to swell for 10min on ice and then lysed by addition of digitonin. Nuclei were pelleted by centrifugation for 5 min at 300 g. The resulting cytosol was cleared by centrifugation for 15min at 1,500 g and finally 60 min at 120,000 g before dialysis overnight against TPB supplemented with 2 mM DTT, 1 mM PMSF and 1 μg/ml each of aprotinin, leupeptin and pepstatin using 8,000 – 10,000 MWCO dialysis tubing. Cytosol concentration was determined by BCA assay. Before each experiment, cytosol was centrifuged at 21,000 g for 5-10 min at 4°C.

Recombinant protein expression and purification

Protein concentrations were determined by their absorbance at 280 nm using their extinction coefficient (ε) predicted by the ProtParam tool. For all assays, 260/280 nm ratios of purified proteins were between 0.6 and 0.85.

GST and GST-DPRs

Expression of GST and GST-DPRs was induced in BL21 and BL21-DE3 Rosetta, respectively, overnight at 16°C using 0.5 mM IPTG.

For GST-DPRs, cells were lysed in DPR-lysis buffer A (20 mM Na_2HPO_4/NaH_2PO_4, pH 7.5, 500 mM NaCl, 1 mM EDTA, 50 mM glutamic acid, 5 mM DTT and 1 μg/ml each of aprotinin, leupeptin hemisulfate and pepstatin A) using sonication and lysozyme. GST-DPRs were purified using GSTrap columns (GE Healthcare). To remove contaminants and RNA from GST-GA_{25} and -PR_{25}, columns were washed stringently with DPR high salt wash buffers of increasing ionic strength (20 mM Na_2HPO_4/NaH_2PO_4, pH 7.5, 50 mM glutamic acid, 2 mM DTT and protease inhibitors containing 1 M NaCl or 2 M NaCl). For GST-GR_{25}, the column was additionally treated with > 250 U/μl benzonase in benzonase buffer (10 mM Na-phosphate pH7.5, 2 mM $MgCl_2$, 2 mM DTT and apo/pep/leu 1 μg/ml each) overnight at 4°C, before applying the washes with DPR high salt buffers as described above. GST-DPRs were eluted in DPR elution buffer (20 mM Na_2HPO_4/NaH_2PO_4, pH 7.5, 150 mM NaCl, 50 mM glutamic acid, 2 mM DTT and protease inhibitors) supplemented with 10-15 mM glutathione and dialyzed against GST-DPR storage buffer (20 mM Na_2HPO_4/NaH_2PO_4 pH 7.5, 150 mM NaCl, 50 mM glutamic acid, 2 mM β−mercaptoethanol). If GST-GR25 was concentrated above 100 μM, a storage buffer containing 0.5 M NaCl was used.

For purification of GST, cells were lysed in DPR lysis buffer B (20 mM Na_2HPO_4/NaH_2PO_4, pH 7.5, 500 mM NaCl, 1 mM EDTA, 2 mM DTT and 1 μg/ml each of aprotinin, leupeptin hemisulfate and pepstatin A as protease inhibitors) using sonication and lysozyme. GST was purified using GSTrap columns (GE Healthcare), washed with DPR wash buffer (50 mM Tris pH7.5, 150 mM NaCl, 2 mM DTT and protease inhibitors) and eluted in wash buffer containing 10 mM glutathione. GST was dialyzed against GST-DPR storage buffer.

(His_6)-TNPO1 and His_6-TNPO3

Recombinant His6-TNPO1 and -TNPO3 were essentially purified as described before for His_6-TNPO1 (Hofweber et al., 2018). In brief, *E. coli* BL21-DE3 Star cells transformed with the respective plasmid were grown for 2-3 days in minimal medium (100 mM KH2PO4, 50 mM K2HPO4, 60 mM Na2HPO4, 14 mM K2SO4, 5 mM MgCl2; pH 7.2 adjusted with HCl and NaOH with 0.1 dilution of trace element solution (41 mM CaCl2, 22 mM FeSO4, 6 mM MnCl2, 3 mM CoCl2, 1 mM ZnSO4, 0.1 mM CuCl2, 0.2 mM (NH4) 6Mo7O24, 17 mM EDTA) supplemented with 6 g of glucose and 3 g of NH4Cl. Subsequently, cells were diluted to an OD_{600} of 0.8 and induced with IPTG to induce protein expression at room temperature for 4-5 h (TNPO1) or overnight at 20°C (TNPO3). His6-tagged proteins were affinity purified using Ni-NTA agarose beads (QIAGEN) equilibrated in 50 mM Tris pH7.5, 150 mM NaCl, 20% (v/v) glycerol, 20 mM imidazole and 2 mM TCEP. Proteins on Ni-NTA were washed with purification buffer containing 1 M NaCl and eluted in buffer supplemented with 500 mM imidazole. Eluted protein was subjected to size exclusion chromatography step in 50 mM Tris-HCl pH 7.5, 150 mM NaCl, 20 mM imidazole, 2 mM TCEP, 20% (v/v) glycerol on a gel filtration column (Hiload 16/600 Superdex 200 pg, GE Healthcare) and subsequently concentrated to 50-140 μM in 20 mM Na_2HPO_4/NaH_2PO_4 pH 8.1, 150 mM NaCl, 5% (v/v) glycerol, 1 mM EDTA, 1 mM DTT.

For polarization experiments, His-tagged TNPO1 was induced for 4-6h at 30°C and affinity purified in 50 mM Tris pH 7.5, 150 mM NaCl, 20 mM imidazole and 2 mM TCEP. Eluted His-TNPO1 was subjected to TEV protease cleavage overnight at 4°C. TEV-cleaved TNPO1 was separated from the His_6-tag using a second step of Ni-NTA purification. The flow-through containing cleaved TNPO1 was subjected to size exclusion chromatography step using a gel filtration column (Hiload 16/600 Superdex 200 pg, GE Healthcare) in 50 mM Tris (pH 7.5), 200 mM NaCl, 2 mM TCEP, 1 mM $MgCl_2$, 5% (v/v) glycerol.

His_6-GFP-TNPO1

His-GFP-TNPO1 was expressed overnight at 18°C in BL21-DE3 Rosetta 2 using 0.35 mM IPTG and purified in 50 mM Tris pH 8, 250 mM NaCl, 2 mM $MgCl_2$ supplemented with 4 mM β-mercaptoethanol and protease inhibitors (1 μg/ml each of aprotinin, leupeptin hemisulfate and pepstatin A) using Ni-NTA agarose (QIAGEN). To remove contaminants, His-GFP-TNPO1 bound to Ni-NTA was washed with purification buffer supplemented with 1 M NaCl and 20 mM imidazole. His-GFP-TNPO1 was eluted in buffer supplemented with 300 mM imidazole and subjected to size exclusion chromatography in 20 mM Na_2HPO_4/NaH_2PO_4 pH 7.5, 75 mM NaCl, 5% (v/v) glycerol, 2 mM DTT and protease inhibitors (1 μg/ml each of aprotinin, leupeptin hemisulfate and pepstatin A). Purified His-GFP-TNPO1 was concentrated to > 100 μM and stored at −80°C.

GST-Tev-TNPO1

Recombinant GST-*Tev*-TNPO1 was purified as described previously (Chook and Blobel, 1999) with modifications. In brief, *E. coli* BL21-CodonPlus(DE3)-RIL cells (Agilent) were transformed with GST-*Tev*-TNPO1 plasmid and expression was induced overnight at 25°C with 1 mM IPTG. Cells were pelleted and resuspended in Tris buffer (50 mM Tris pH 7.5, 100 mM NaCl, 1 mM EDTA, 20% (v/v) glycerol, 2 mM DTT, supplemented with protease inhibitors), then lysed by sonication. Cell lysate was then loaded onto glutathione Sepharose™ 4 Fast Flow resin (GE Healthcare), and washed with Tris buffer, followed by ATP buffer (50 mM Tris pH 7.5, 100 mM NaCl, 1 mM EGTA, 0.5 mM $MgCl_2$, 5 mM ATP, 20% glycerol, 2 mM DTT, supplemented with protease inhibitors), then washed and eluted with Buffer A (20 mM imidazole, 75 mM NaCl, 1 mM EDTA, 20% (v/v) glycerol, 2 mM DTT). Finally, the protein was cleaved with Tev protease and purified on a HiTrap Q HP column (GE Healthcare) using a salt gradient. Purified protein was concentrated, flash frozen, and stored at −80°C.

His_6-S-Impβ and His_6-GFP-Impβ

For expression of His-S-Impβ, BL21-DE3 Rosetta2 transformed with the respective expression plasmid were grown to OD_{600}∼1.2 and diluted to OD_{600} ∼0.6 using ice cold medium and supplemented with 30 mM K_2HPO_4 and 2% EtOH before addition of 0.3-0.5 mM IPTG overnight at 18°C. His-S-Impβ was purified in Talon buffer (50 mM Tris pH 8, 250 mM NaCl, 2 mM $MgCl_2$, 10% (v/v) glycerol, 20 mM imidazole supplemented with 4 mM β-mercaptoethanol and 1 μg/ml each of aprotinin, leupeptin hemisulfate and pepstatin A using Ni-NTA agarose (QIAGEN). To remove contaminants, His-S-Impβ bound to Ni-NTA was washed in lysis buffer supplemented with 1M NaCl after an optional washing step with 20 mM imidazole, 10 mM ATP and 5 mM $MgCl_2$ in presence of denatured protein. His-S-Impβ was eluted in lysis buffer supplemented with 300 mM imidazole and subjected to size exclusion chromatography (Hiload 16/600 Superdex 200 pg, GE Healthcare) in 20 mM Na_2HPO_4/NaH_2PO_4 pH7.5 or pH8, 75 mM NaCl, 5% (v/v) glycerol, 2 mM DTT and 1 μg/ml each of aprotinin, leupeptin hemisulfate and pepstatin A. If required, purified Impβ was concentrated to > 150 μM.

His_6-Impα1 and His_6-Impα3

Expression of His-Impα1 and -Impα3 were induced in BL21-DE3 Rosetta-LysS or BL21-DE3 Rosetta, respectively, using 0.5 mM IPTG at OD_{600} ∼0.8 for ∼5h or at 18°C overnight. Purification of His-Impα1 was performed in 20 mM Tris pH7.5, 600 mM NaCl supplemented with 4 mM β−mercaptoethanol, 1 mM PMSF and 1 μg/ml each of aprotinin, leupeptin hemisulfate and pepstatin A using HisTrap columns. For His-Impα3, 50 mM Tris pH7.5, 600 mM NaCl, 0.2% Tween-20 supplemented with 4 mM β−mercaptoethanol, 1 mM PMSF and 1 μg/ml each of aprotinin, leupeptin hemisulfate and pepstatin A was used. The protein on the column was washed with the respective lysis buffer (lacking Tween-20) supplemented with increasing imidazole concentrations (10 mM, 12 mM, 15 mM) before elution using buffer containing 600mM imidazole. Finally, size exclusion chromatography (Hiload 16/600 Superdex 200 pg, GE Healthcare) was performed in 50 mM Tris pH7.5, 250 mM NaCl, 0.8 mM PMSF, 2mM DTT, 1 μg/ml each of aprotinin, leupeptin hemisulfate and pepstatin A (Impα1) or 50 mM Tris pH7.5, 150 mM NaCl, 1 mM PMSF, 4 mM β-mercaptoethanol, 1 μg/ml each of aprotinin, leupeptin hemisulfate and pepstatin A (Impα3). If required, the protein was concentrated to ≥ 100 μM.

CRM1

His_{10}-ZZ-CRM1 was induced in BL21-DE3 Rosetta2 overnight at 18°C using 0.5 mM IPTG. Cells were lysed in 50 mM Tris pH7.4, 500 mM NaCl, 1 mM EDTA, 2 mM $MgCl_2$, 2 mM imidazole supplemented with 4 mM β−mercaptoethanol, 1 μg/ml each of aprotinin, leupeptin hemisulfate and pepstatin A and 0.1 mg/ml RNase A using lysozyme and sonication. His-ZZ-CRM1 was purified using Ni-NTA agarose (QIAGEN). After several washes with CRM1 buffer A (50 mM Tris pH7.4, 500 mM NaCl, 2 mM $MgCl_2$, 2 mM imidazole, 4 mM β-mercaptoethanol, 1 μg/ml each of aprotinin, leupeptin hemisulfate and pepstatin A), His-ZZ-CRM1 was eluted by CRM1 buffer A with 300 mM imidazole. The His-ZZ-tag was cleaved off during overnight dialysis against 20 mM Na_2HPO_4/NaH_2PO_4 pH7.4, 75 mM NaCl, 5% (v/v) glycerol, 2 mM DTT using His-Tev protease. Cleaved CRM1 was separated from both His-ZZ tag and protease using size exclusion chromatography (Hiload 16/600 Superdex 200 pg, GE Healthcare) in dialysis buffer and subsequently concentrated to ≥ 70 μM.

TDP-43-Tev-MBP-His_6

TDP-43-MPB-His_6 was purified with minor amendments according to Wang et al. (2018). In brief, protein expression was performed in *E. coli* BL21-DE3 Rosetta 2 or BL21-codonPlus (DE3)- RIL cells (Agilent) using 0.5 mM or 0.1 mM IPTG, respectively, overnight at 16°C.

For visualization of TDP-43 phase separation by microscopy or sedimentation analysis, cells were lysed in purification buffer (20 mM Tris pH 8, 1 M NaCl, 10 mM imidazole, 10% (v/v) glycerol, 4 mM β-mercaptoethanol and 1 μg/ml each of aprotinin, leupeptin hemisulfate and pepstatin A) supplemented with 0.1 mg/ml RNase A using lysozyme and sonication. For turbidity assays, cells were resuspended in purification buffer (20 mM Tris pH 8.0, 1 M NaCl, 10 mM imidazole, 10% (v/v) glycerol, 2 mM β-mercaptoethanol supplemented with complete EDTA-free protease inhibitor cocktail) and lysed using lysozyme and sonication. Protein was purified by Ni-NTA agarose (QIAGEN) and eluted using 300 mM imidazole in purification buffer. For all microscopy-based assays or sedimentation analysis, full length TDP-43-MBP-His_6 was separated from protein aggregates and contaminants by size exclusion chromatography (Hiload 16/600 Superdex 200 pg, GE Healthcare) in 20 mM Tris pH 8, 300 mM NaCl, 10% (v/v) glycerol supplemented with

2 mM DTT. For turbidity measurements, TDP-43-MBP-His_6 was further purified over amylose resin (NEB) and eluted with 20 mM Tris-HCl, pH 8.0, 1 M NaCl, 10 mM imidazole, 10 mM maltose, 10% (v/v) glycerol, and 1 mM DTT. Purified protein was concentrated, flash frozen and stored at −80°C.

MBP- Tev-TDP-43-GFP-Tev-His_6

Expression was induced in BL21-DE3 Rosetta2 using 1 mM IPTG overnight at 15°C. The protein was purified by tandem-affinity purification using Ni-NTA agarose (QIAGEN) and amylose resin (NEB). First, cells were lysed in resuspension buffer (50 mM Na_2HPO_4/NaH_2PO_4 pH 8.0, 300 mM NaCl, 10 μM $ZnCl_2$, 10% (v/v) glycerol, 40 mM imidazole, 4 mM β-mercaptoethanol and protease inhibitor cocktail (Sigma)) using sonication. The protein was bound to Ni-NTA agarose, washed with resuspension buffer lacking glycerol and eventually eluted in resuspension buffer including 250 mM imidazole. For binding to amylose beads, the eluate was diluted to 150 mM NaCl and after several washes with binding buffer eluted in 40 mM HEPES pH 7.5, 300 mM NaCl, 5% (v/v) glycerol, 1 mM DTT and protease inhibitors containing 20 mM maltose. MBP-TDP-43-GFP-His_6 was stored in 40 mM HEPES pH 7.5, 300 mM NaCl, 5% (v/v) glycerol, 1 mM DTT and protease inhibitors.

His_6-Tev

Expression and purification was performed as described in Hofweber et al. (2018). In brief, expression was induced in BL21-DE3 Rosetta-LysS overnight at 20°C using 1 mM IPTG. Cells were lysed in 50 mM Tris pH8, 200 mM NaCl, 20 mM imidazole, 10% (v/v) glycerol, 4 mM β-mercaptoethanol and 1 μg/ml each aprotinin, leupeptin and pepstatin in presence of 0.1 mg/ml RNase A using lysozyme and sonication. His-Tev was purified using Ni-NTA agarose (QIAGEN), washed using lysis buffer containing 1 M NaCl and eluted in lysis buffer at pH 8.5 supplemented with 800 mM imidazole. His_6-Tev was dialyzed against storage buffer (50 mM Tris, 150 mM NaCl, 20% glycerol, 2 mM DTT).

Biotin-DPR Pulldowns

For pulldowns (PDs) using biotin-labeled DPR peptides as bait, Streptavidin Sepharose HP (GE Healthcare) was blocked with 20 mg/ml chicken ovalbumin in B-buffer (50 mM Tris pH 7.5, 200 mM NaCl, 1 mM $MgCl_2$, 5% (v/v) glycerol supplemented with 2 mM DTT and protease inhibitors), before biotin-labeled DPRs were immobilized overnight in presence of 2 mg/ml ovalbumin in B-buffer (5 μg peptide per reaction on 10 μl bead volume). For the actual pulldown, 5 μg of prey protein per reaction was added to immobilized biotin-DPRs in B-buffer with 2 mg/ml BSA (50 mM Tris pH 7.5, 200 mM NaCl, 1 mM $MgCl_2$, 5% (v/v) glycerol supplemented with 2 mM DTT and protease inhibitors). After several washes in B-buffer lacking BSA, bound proteins were eluted from the beads using two-fold concentrated protein loading buffer (125 mM Tris pH 6.8, 20% (v/v) glycerol, 4% (w/v) SDS, 0.05% (w/v) bromophenolblue, 2% (v/v) β-mercaptoethanol) and visualized by SDS-PAGE and Sypro-Ruby (Sigma) stain. PDs were performed $\geq$ 2 times as independent replicates.

Fluorescence Polarization Measurements

For this assay, N-terminally fluorescein isothiocyanate (FITC)-labeled GR_{25} and PR_{25} peptides were used at 250 nM. All protein samples were equilibrated in 50 mM Tris (pH 7.5), 200 mM NaCl, 2 mM TCEP, 1 mM $MgCl_2$, 5% (v/v) glycerol. Measurements were taken at room temperature in black 384-well plates using a ClarioStar Plus (BMG labtech) spectrophotometer. Filters were selected as a function of FITC optical characteristics (λ_{ex} = 495 nm, and λ_{em} = 530 nm). 250 nM FITC-GR_{25} and FITC-PR_{25}, respectively, was incubated with increasing concentration of purified TNPO1 in a final volume of 35 μl. The polarization data were fitted using CLARIOstar - Data Analysis (MARS) to the following equation:

$$P = P_0 + (P_{max} * L)/(L + k_D)$$

Here, P_0 represents the polarization of FITC-GR_{25} and FITC-PR_{25} in absence of TNPO1, and P_{max} to the highest polarization of the binding curve corresponding to the saturation of the interaction. L corresponds to the concentration of TNPO1 protein and k_D is the dissociation constant.

SAXS

For this assay, N-terminally fluorescein isothiocyanate (FITC)-labeled GR_{25} and PR_{25} peptides were used. All samples were equilibrated in 50 mM Tris (pH 7.5), 200 mM NaCl, 2 mM TCEP, 1 mM MgCl2, 5% (v/v) glycerol. SAXS data for solution of the TNPO1-$[GR]_{25}$ and TNPO1-$[PR]_{25}$ complexes were recorded with an *in-house* SAXS instrument (SAXSspace, Anton Paar, Graz, Austria) equipped with a sealed X-ray tube source and a one-dimensional Mythen2 R 1k hybrid photon coupling detector (Dectris, Baden-Daettwil, Switzerland). The scattering patterns were measured with a 90-minutes exposure time (90 frames, each 1 minute) with a solute concentration of 50 μM (TNPO1) at 4°C. Radiation damage was excluded on the basis of a comparison of individual frames of the 90-minutes exposures, wherein no changes were detected. A range of momentum transfer of $0.010 < s < 0.63$ Å^{-1} was covered ($s = 4\pi \sin(\theta)/\lambda$, where 2θ is the scattering angle, and λ is the X-ray wavelength, in this case 1.5 Å.

All SAXS data were analyzed and processed using the SAXS analysis package (Anton Paar, version 3.0). The data were desmeared using GIFT (PCG-Software). The interatomic distance distribution function (P(r)) were computed with GIFT (PCG-Software).

In vitro phase separation assays

For all assays, the investigated protein or cytosol was centrifuged for 5-10 min at 4°C and 21,000 g to remove any preformed protein precipitates.

Sedimentation assay

For sedimentation analysis of NTRs, 1 μM purified NTR (or 500 nM Impα with 500 nM Impβ) was incubated in the absence or presence of indicated amounts of TMR-labeled DPRs

in 50 μL condensation buffer (50 mM Tris pH 7.5, 200 mM NaCl, 2 mM DTT) for 15 min at 4°C, followed by centrifugation for 15 min at 21,000 g at 4°C. For quantitative sedimentation analysis of TDP-43, 1 μM of purified TDP-43-MBP-His was cleaved in the absence or presence of equimolar amounts of GST-tagged DPRs and/or NTRs using 20 μg/ml His-Tev for 60 min at 30°C, followed by centrifugation for 15 min at 21,000 g at 4°C. Equal volumes of supernatant and pellet fraction were analyzed by SDS-PAGE and proteins visualized by Sypro-Ruby stain or western blot.

For sedimentation analysis of proteins from HeLa cytosol, cytosol was used at 1 mg/ml in TPB (20 mM HEPES pH 7.3-7.4, 110 mM K-Ac, 2 mM $Mg(Ac)_2$, 1 mM EGTA supplemented with protease inhibitors and 2mM DTT). Indicated concentrations of TMR-labeled DPRs were added and reactions incubated for 15 min at 4°C before centrifugation at 21,000 g for 15min. Equal volumes of pellet and supernatant were analyzed by western blot analysis.

Visualization of condensates by microscopy

To visualize condensation of GFP-TNPO1 by R-rich DPRs, 1 μM purified His-GFP-TNPO1 or GFP-Impβ (in absence or presence of equimolar amounts of unlabeled His-Impα3) was incubated with indicated concentration of TMR-labeled DPRs in droplet buffer A (20 mM Na_2HPO_4/NaH_2PO_4, pH 7.5, 200 mM NaCl, 2.5% (v/v) glycerol, 1 mM DTT). To follow TDP-43 condensate formation, 2 μM TDP-43-MBP-His mixed with substoichiometric amounts of MBP-TDP-43-GFP-His (ratio 1:4-1:5) was cleaved in the absence or presence of TMR-labeled DPRs at indicated concentrations using 100 μg/ml His-Tev in condensation buffer (50 mM Tris pH 7.5, 200 mM NaCl, 2 mM DTT). For shielding by NTRs, TDP-43-*Tev*-MBP/ MBP-*Tev*-TDP-43-GFP was mixed with equimolar concentration of TMR-GR_{25} in absence or presence of NTRs before Tev-cleavage. Condensates were imaged in 384 well plates using a laser scanning confocal microscope. For RNA-induced condensate formation of TMR-GR_{25}, total RNA was heated for 1 min at 65°C and chilled on ice before adding it to a final concentration of 20 ng/μl to 20 μM TMR-GR_{25} in the absence or presence of equimolar concentrations of NTRs in 20 mM Na_2HPO_4/NaH_2PO_4 pH7.5, 200 mM NaCl, 2.5% (v/v) glycerol and 2 mM DTT.

For analysis of GR-induced GFP-TNPO1 condensates by FRAP, 2μM GFP-TNPO1 were incubated with 20μM TMR-GR_{25} for 1-2 h at RT in a microscopic chamber before FRAP analysis.

Analysis of oligomer formation by SDD-AGE

Samples were prepared in protein low binding tubes (Eppendorf) using 2 μM importin and 20 μM TMR-DPR in 50 mM Tris pH 7.5, 200 mM NaCl supplemented with 1x protease inhibitor mix (Sigma) and 1 mM TCEP. After 1 h incubation at RT, samples were analyzed by SDD-AGE (modified protocol according to French et al. [2019] and Halfmann and Lindquist [2008]) in SDD-AGE buffer (40 mM Tris-HCl pH 6.8, 5% Glycerol, 0.5% SDS, 0.1% bromphenol blue) on a horizontal 1.5% agarose gel in running buffer (60 mM Tris, 20 mM Acetate, 200 mM glycine, 1 mM EDTA and 0.1% SDS) for 5-6 h at low voltage. Proteins are transferred on nitrocellulose membrane using capillary transfer in TBS (50mM Tris pH 7.6, 150mM NaCl) overnight at 4°C and subsequently processed according to western blot standard protocol.

Turbidity assay

Purified TDP-43-MBP-His and TNPO1 were first thawed and buffer exchanged into 20 mM HEPES-NaOH, pH 7.4, 150 mM NaCl and 1 mM DTT, using a Micro Bio-Spin™ P-6 Gel Column (Bio-Rad). TDP-43-MBP-His was then diluted to a final concentration of 5 μM, with addition of either 2 μM GR_{20} (or equivalent volume of 1x PBS as a control), 5 μM TNPO1, or addition of both. Phase separation was initiated by addition of 1 μg/ml Tev protease and measured over 16 h at an absorbance of 395 nm using a TECAN M1000 plate reader. Values were normalized to TDP-43 + Tev protease alone to determine the relative extent of phase separation.

Solubility assay of endogenous TDP-43 by RIPA extraction

HeLa cells ($0.5\text{-}1x10^6$) were incubated with 10 μM TMR-DPRs (in medium lacking serum) for 2h and then harvested by scraping into PBS and centrifugation at 1,200 g for 5 min. The cell pellet was resuspended in 200 μl RIPA buffer (50 mM Tris-HCl, pH 8.0, 150 mM NaCl, 1% NP-40, 0.5% deoxycholate, 0.1% SDS) supplemented with ~0.05U/μl benzonase (Sigma), 1x Sigma protease inhibitor mix and 1x phosphatase inhibitors (final concentration: 10 mM NaF, 1 mM β-glycerophosphate, 1 mM Na_3VO_4) and incubated on ice for 10-15 min. Cells were sonicated once for 45 s using a BioRuptorPico (Diagenode) and 10% of the lysate retained for the input. The rest of the lysate was centrifuged for 30 min at 13,000 g and 4°C to separate the RIPA-soluble proteins from the insoluble proteins. The RIPA insoluble pellet was resuspended and washed once in RIPA buffer, followed by 45 s sonication in the BioRuptorPico and subsequent centrifugation at 13,000 g for 30 min at 4°C. The RIPA insoluble pellet was finally lysed in 40 μl Urea buffer (7 M urea, 2 M thiourea, 4% CHAPS, 30 mM Tris-HCl, pH 8.5) and 45 s sonication using the BioRuptorPico. Samples were analyzed by anti-TDP-43

western blot. Note that the 4.5x overrepresentation of the pellet fraction for reasons of visibility in the western blot was corrected in the quantification.

Immunocytochemistry

HeLa cells grown on No. 1.5 coverslips were fixed in 3.7% formaldehyde/PBS buffer for 7-10 min at RT. Permeabilization was performed using 0.5% (v/v) TX-100/PBS for 5 min at room temperature. Cells were subsequently blocked in blocking buffer (at least 10 min in 1% donkey serum in PBS/ 0.1% Tween-20) and incubated with primary antibodies in blocking buffer for 1-2 h at RT or overnight at 4°C. Secondary antibodies were diluted 1:1000 in blocking buffer and incubated for 30-60 min at room temperature. Three washing steps after each antibody incubation were performed using PBS/ 0.1% Tween-20. DNA was stained with DAPI at 0.5 μg/ml in PBS and cells mounted in ProLong Diamond Antifade.

Nuclear transport assay (Hormone-induced import assay)

To analyze import of GCR_2-GFP_2 tagged (MBP-)cNLS or TDP-43 reporters, HeLa cells were grown for at least 2 passages in DMEM supplemented with 10% dialyzed FBS. Cells were either left untreated (control) or pre-incubated for 2h with 10μM TMR-labeled GR_{25} or PR_{25} added once directly into the imaging medium (fluorobrite without serum). Import of the GCR_2-GFP_2-reporter was induced by adding dexamethasone (5 μM final concentration) in imaging medium and followed by live cell imaging using a spinning disk confocal microscope. Images were acquired for a duration of 40-50 min in 2.5 min intervals. Successful uptake of the peptide was validated before start of the experiment and only cells displaying efficient peptide uptake in form of cytoplasmic (and/or nuclear) TMR signal were subsequently quantified.

MICROSCOPY

Laser scanning confocal microscopy

Confocal microscopy of HeLa cells and condensates of recombinant proteins was performed at the Bioimaging core facility of the Biomedical Center with an inverted Leica SP8 microscope, using lasers for 405, 488, 552 and 638 nm excitation. For fixed cells, images were acquired using two-fold frame averaging with a 63x1.4 oil objective and an image pixel size of 59 nm. The following fluorescence settings were used for detection: DAPI: 419-442 nm, GFP: 498-533 nm, Alexa 555: 562-598 nm, Alexa 647: 650-700 nm. Recording was performed sequentially to avoid bleed-through using a conventional photomultiplier tube (PMT). Unless otherwise noted, images of condensates were acquired without averaging. For DPR-induced condensation of GFP-TNPO1 or TDP-43, a 63x/1.4 oil objective was used with an image pixel size of 70-71 nm. For condensates of TMR-GR_{25} in presence of RNA or TDP-43 with NTRs, a 100x/1.4 oil objective was used with a pixel size of 80 nm and 70 nm respectively. Recording, if applicable, was performed sequentially using a PMT with the following settings: GFP: 498-520 nm, TMR: 562-615 nm. For images of condensate formation of TDP-43 in the presence of NTRs, two-fold frame averaging with the following PMT settings: GFP: 498-533.

Spinning disc confocal live cell microscopy

Live cell imaging was performed at 36.5°C and 5% CO_2 (EMBLEM environmental chamber) using an inverted microscope (Axio Observer.Z1; Carl Zeiss, Oberkochen, Germany) equipped with a confocal spinning disc (CSU-X1; Yokogawa, Tokyo, Japan) and a 63x/1.4 oil immersion lens. Images were acquired using the 488 nm SD laser line and an EM-CCD camera (EvolveDelta; Photomoetrics) at bin 1x1. For photobleaching, a laser scanning device (UGA-42 Geo; Rapp OptoElectronic, Hamburg, Germany) was used, allowing for simultaneous laser illumination within hardware-defined shapes of different sizes.

Fluorescence Recovery after Photobleaching (FRAP)

Experiments were performed on an inverted microscope (Axio Observer.Z1; Carl Zeiss, Oberkochen, Germany) equipped with a confocal spinning disc (CSU-X1; Yokogawa, Tokyo, Japan) and a 100x/1.46/Ph3 (TNPO1 Condensates) or 63x/1.4 (live cells) oil immersion lens. For localized photobleaching, a laser scanning device (UGA-42 Geo; Rapp OptoElectronic, Hamburg, Germany) was used. The ''Geo'' module allowed for simultaneous laser illumination within hardware-defined shapes of different sizes. Here, a square-like shape with an illumination size of ~5 μm (TNPO1 condensates) or 10 μm (cytoplasmic FRAP) in the sample was selected. For each experiment, the initial fluorescence intensity was bleached to ≥30% of the initial intensity using a 473 nm diode laser (DL-473/75; Rapp OptoElectronic, Hamburg, Germany). For live cells, images were acquired in the streaming mode using the 488 nm SD laser line and an EM-CCD camera (EvolveDelta; Photomoetrics) at bin 1x1. Fluorescence recovery of ≥ 14 bleached condensates was recorded at RT using streaming mode for 1 min followed a block of 4 min with image acquisition in 15 s intervals in two independent experiments.

QUANTIFICATION AND STATISTICAL ANALYSIS

Microscopy

Laser scanning confocal images were acquired using LAS X (Leica), live cell images were acquired in ZEN2 (Zeiss). All images were processed using ImageJ/Fiji software applying linear enhancement for brightness and contrast. For quantification of size

of RNA/TMR-GR_{25} condensates in absence or presence of NTRs, confocal images were analyzed using ImageJ/Fiji. Images were displayed in gray values and a median filter with radius 2 applied. A threshold providing best coverage of condensates was set identically to all images within one experiment using the default setting built into Fiji/ImageJ and allowing for detection of white objects on black background. Subsequently a particle analysis was performed excluding particles < 0.1.

Statistical analyses were performed in GraphPad Prism 8, details are given in each figure legend.

FRAP analysis of cytoplasmic GCR_2-GFP_2 dynamics

Intensities of bleached areas were corrected both for bleaching due to imaging over time and background noise. The corresponding calculations were performed with the FIJI/ImageJ macro ''TimeSeries Analyzer'' by calculating the fluorescence intensity over time (I(t)) as follows:

$$I(t) = [ROI1(t) - ROI3(t)]/[ROI2(t) - ROI3(t)]$$

with ROI1 giving the averaged gray values within the center of the bleached area, and ROI2 corresponds to the averaged gray values of the total cell. ROI3 corresponds to averaged background values. Obtained values were further normalized to the initial fluorescence by dividing I(t) by the mean gray value of the first image before bleaching (t = 0).

Densitometry measurements (Sypro-Ruby, western blot)

To determine the solubility of NTRs, TDP-43 or GST-GR_{25}, by quantitative sedimentation analysis, densitometry measurements of band intensities of supernatant and pellet fractions were performed after Sypro-Ruby gel staining or western blot analysis. For this, implemented plugins in the corresponding gel detection software for Sypro-Ruby staining (Image Lab Software; Bio-Rad Laboratories) or western blot (Image Studio Software; Li-Cor) were employed. To determine the solubility of individual proteins, the relative amount of the respective protein in the supernatant was calculated as percent of the total (i.e., sum of supernatant and pellet). All statistical analyses were performed in GraphPad Prism 8 and details indicated in the respective figure legends.